

A three-dimensional simulation and process analysis of tropospheric Ozone Depletion Events (ODEs) during the springtime of Arctic using CMAQ

Simeng Li¹, Le Cao¹, Yicheng Gu¹, and Yuhan Luo²

¹Key Laboratory for Aerosol-Cloud-Precipitation of China Meteorological Administration, Nanjing University of Information Science and Technology, Nanjing, 210044, China

²Key Laboratory of Environmental Optics and Technology, Anhui Institute of Optics and Fine Mechanics, Chinese Academy of Sciences, Hefei, 230031, China

Correspondence: Le Cao (le.cao@nuist.edu.cn)

Abstract. The tropospheric Ozone Depletion Event (ODE), first observed at Barrow (now known as Utqiagvik), Alaska, is a phenomenon that frequently occurs during the springtime of the Arctic. In ~~the present this~~ study, we performed a three-dimensional model study on ODEs occurring at Barrow and its surrounding areas between ~~March 28th and April 6th~~ 28 March and 6 April, 2019, using a 3-D multi-scale air quality model, CMAQ. Several ODEs observed at Barrow were ~~successfully~~ captured, and two of them were ~~analyzed thoroughly using process analysis~~ thoroughly analyzed using the process analysis method to estimate the contributions of horizontal transport, vertical transport, dry deposition and the overall chemical process to the variations of ozone and bromine species during ODEs. We found that the ODE occurring between ~~30 and 31~~ 30th and 31st, 2019 (referred to as ODE1) was ~~caused mainly by a~~ primarily caused by the horizontal transport of ~~an ozone-lacking a low-ozone~~ air from the Beaufort ~~sea~~ Sea to Barrow. ~~This ozone-lacking air was formed due~~ The formation of this low-ozone air over the sea was largely attributed to a release of sea-salt aerosols from the Bering Strait under ~~a strong wind condition, resulting strong~~ strong wind conditions, stemming from a cyclone generated ~~at on~~ at the Chukotka Peninsula. It was also ~~found that over the Beaufort sea, the surface ozone drops to a level lower~~ discovered that the surface ozone dropped to less than 5 ppb over the Beaufort sea, and the ~~local chemistry contributed as large as overall chemical process contributed up to~~ 10 ppb to the ozone loss. Moreover, BrO over the sea ~~was found to attain~~ reached a maximum of approximately ~~100~~ 80 ppt. ~~This ozone-lacking low-ozone~~ air over the sea was ~~then~~ then horizontally transported to Barrow, leading to the occurrence of ODE1. Regarding another ODE on ~~April 2nd~~ 2 April (ODE2), we found its occurrence also dominated by the horizontal ~~advection~~ transport from the sea, but under the control of an anti-cyclone. The termination of this ODE was ~~mainly~~ mainly attributed to the ~~replenish~~ replenishment of ozone-rich air from the free troposphere by a strong vertical transport.

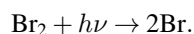
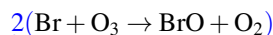
1 Introduction

Ozone, one of the most important atmospheric ~~constituent~~ constituents in the atmosphere of the Arctic, has historically attracted much attention from the scientific community. ~~In the Arctic, due to the lack of human activities, The background level of ozone in the Arctic is approximately 40-60 ppb (parts per billion by volume) (Seinfeld and Pandis, 2016), and the long-range transport~~

of anthropogenic emissions of ozone precursors from North America and East Asia generally increases the tropospheric ozone ~~remains at a background level, 40-60 ppbv (Seinfeld and Pandis, 2016)~~in the Arctic since the 1990s (Sharma et al., 2019).

25 However, Oltmans (1981) observed an abnormal decrease ~~of~~in surface ozone at Barrow (now known as Utqiagvik, 71.3230° N, 156.6114° W), Alaska in the springtime. The surface ozone was found to drop from the background level to a few ~~ppbv~~ppb, within a couple of days or even hours, which is commonly called ozone depletion events (ODEs~~for short~~).

After that, Barrie et al. (1988) found that the tropospheric ~~ODE is~~ODEs are formed due to the occurrence of an auto-catalytic reaction cycle involving bromine chemistry, of which the major reactions are shown below (Barrie et al., 1988; Platt
30 and Hönninger, 2003; von Glasow and Crutzen, 2014):



35 Net : $2\text{O}_3 \rightarrow 3\text{O}_2$.

In this reaction cycle, the total amount of ~~Br and BrO keeps~~bromine stays constant, which means ~~that these bromine species play as catalysts~~the bromine plays as a catalyst for the ozone depletion. Aside from reaction cycle (I), Br and BrO can also react with HO₂ radicals, forming HBr and HOBr, respectively. HBr and HOBr are relatively inert, so ~~that~~ the formation of these two species tends to terminate the reaction cycle. HBr can also be generated from reactions between Br atoms and olefins or
40 aldehydes(~~Platt and Hönninger, 2003~~), then leaves the atmosphere due to its tendency to dissolve (Platt and Hönninger, 2003).

However, heterogeneous reactions taking place at the surface of substrates (such as frost flowers or sea-salt aerosols) lead to the liberation of ~~the~~ inert bromine (McConnell et al., 1992; Fan and Jacob, 1992), which is essential for the ~~re-emissions~~re-emission of bromine, the so-called “bromine explosion” mechanism (Platt and Lehrer, 1997; Wennberg, 1999). Reaction (R1) represents one of these heterogeneous reactions, which forms active Br₂ from bromine ions (Br⁻):



Also, a similar heterogeneous reaction involving Cl⁻ also occurs:



~~to form~~forming another active bromine species, BrCl. Therefore, additional bromine can be rapidly released into the atmosphere, causing a fast ozone depletion in the boundary layer. Under this condition, the ~~major~~dominant oxidant in the atmosphere shifts from ~~ozone~~OH, the major product of ozone photolysis, to bromine species. Because the bromine species are
50 capable of accelerating the deposition of mercury from the air, more mercury can enter ~~into~~ the ocean, and then influence the biosphere through marine wildlife (Simpson et al., 2007; Steffen et al., 2008).

Many researchers have contributed to the study of ODEs. ~~Observations and experiments were made to establish the~~ The internal relationship between the ozone depletion and the bromine explosion. ~~Moreover, scientists also tried~~ was established through observations and experiments (Oltmans, 1981; Barrie et al., 1988; Bottenheim et al., 1990; McConnell et al., 1992; Fan and Jacob, 1992; F
55 Furthermore, scientists attempted to reproduce ODEs using through parameterizations or model simulations. To name a few, Lehrer et al. (2004) used ~~an a~~ one-dimensional model to identify weather conditions and underlying surface properties necessary for the occurrence of ODEs. They concluded that the sunlight, bromine-containing surface, and strong conversion on the top of the boundary layer are essential conditions for the occurrence of ODEs. ~~Only in spring can these conditions~~
60 ~~be satisfied~~ These requirements can only be met in the springtime, which is the main reason that ODEs ~~were are~~ mostly observed in ~~the springtime. Thomas et al. (2011, 2012) studied~~ spring. Thomas et al. (2011, 2012) used a one-dimensional atmospheric boundary layer model named MISTRA-SNOW to study the chemistry on the snow at Summit, Greenland ~~using a one-dimensional atmospheric boundary layer model named MISTRA-SNOW~~. They concluded that the bromine- and nitrate-containing surfaces help to maintain the concentrations of NO and BrO during the study time.

70 The first three-dimensional simulation of ODEs was implemented by Zeng et al. (2003, 2006), who found ~~approximately 60% of the northern high altitudes covered by a~~ that low surface ozone (<20 ppbv) ~~and a high BrO. Zeng et al. ppb) and high~~ BrO were present in about 60% of the northern high-altitude region. Zeng et al. (2006) also concluded that there exists a strong anti-correlation between the tropospheric BrO and the surface temperature. Besides, they found that the concentration of BrO is relevant to movements of air masses and the variation of ~~the~~ temperature rather than the absolute value of the
75 temperature. Later, by using a global chemistry transport model, p-TOMCAT, Yang et al. (2008, 2010, 2019) proposed that the bromine in polar area mostly comes from sea-salt aerosols. A release of active bromine into the atmosphere then results in an average of 8% of the tropospheric ozone loss.

Recently, Herrmann et al. (2021, 2022) and Marelle et al. (2021) tried to reproduce ODEs using a mesoscale forecasting model WRF-Chem. These studies are a major advance in 3-D simulations of ODEs. In the study of ~~Herrmann et al.~~ Herrmann et al. (2021),
75 they concluded that the bromine explosion mechanism alone is unable to maintain enough BrO. Instead, a heterogeneous reaction involving ozone and bromine ions makes the bromine explosion possible. Moreover, ~~Marelle et al.~~ Marelle et al. (2021) found that the surface snow and blowing snow are both able to initialize the ODEs. It was suggested by ~~Marelle et al.~~ Marelle et al. (2021) that, although blowing snow is the major source of sea-salt aerosols, it only exerts a weak impact on ODEs. Both ~~of these two~~ studies contribute largely to the 3-D simulations of ODEs.

80 However, in previous simulations of ODEs, due to the use of self-constructed chemical mechanisms without validations, uncertainties may be induced into chemical simulations. Moreover, contributions of physical and chemical processes to the occurrence of ODEs need to be studied more thoroughly. Therefore, in this study, we conducted simulations of ODEs using a 3-D multi-scale air quality model, CMAQ (Community Multiscale Air Quality Modeling System), focusing on Barrow and surrounding areas (see Fig. 1a). We also used a validated chemical mechanism originally ~~instrumented~~ implemented in CMAQ,
85 CB05eh51_ae6_aq, which ~~considers~~ includes the halogen chemistry (Sarwar et al., 2015; Sherwen et al., 2016; Yarwood et al., 2012). In addition, we performed a process analysis (Gipson, 1999) to estimate the contribution ~~from~~ of each physical or

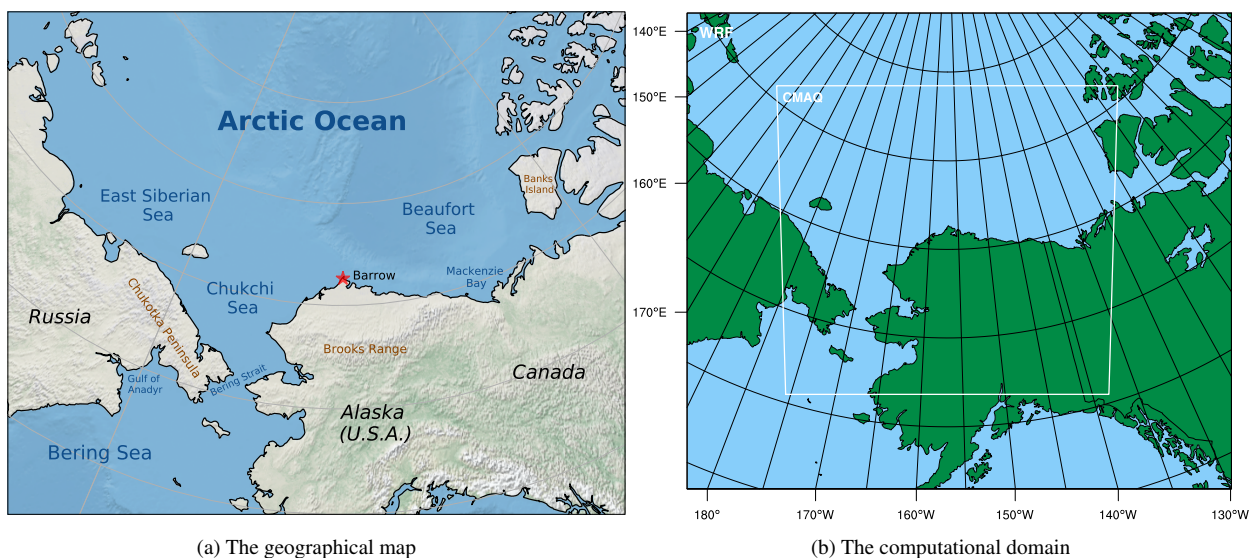


Figure 1. The geographical map of the research area and the computational domain used in WRF and CMAQ. [The red asterisk in the figure denotes the location of Barrow.](#)

chemical process to the variations of ozone and bromine species during ODEs. By doing that, we were able to quantitatively analyze the variations of [the](#) selected species and [evaluate](#) the importance of influencing factors for ODEs.

In the following sections, we will introduce the configurations of our simulations in Sect. 2, and then present the validations and quantitative analysis of two ODEs in Sect. 3. At last, conclusions and future work are given in Sect. 4.

2 [Observational Data Measurements](#) and Model Settings

In this study, the CMAQ model (US EPA Office of Research and Development, 2018) was used to reproduce the ODEs. The WRF model (Weather Research and Forecasting, Skamarock et al., 2008) was used to capture the meteorological parameters and drive the CMAQ model. Hourly [observational data measurements](#) of in-situ meteorological parameters and ozone were also used to validate the simulations.

2.1 Model Settings

CMAQ requires the input of meteorological fields including temperature, wind and pressure to drive the chemical simulations. In this study, outputs of WRF model were used to drive the CMAQ model.

Table 1. Configurations of WRF and CMAQ in the present study.

Options	Settings	References
WRF		
Microphysics	Thompson scheme	Thompson et al. (2008)
Boundary-layer model	Mellor-Yamada-Janjic scheme	Janjić (1994)
Land surface model	Noah land-surface model	Chen et al. (1997)
Surface-layer model	Monin-Obukhov (Janjic Eta) similarity scheme	Janjić (1994)
Cumulus parametrization	Modified Tiedtke scheme	Tiedtke (1989)
Longwave radiation	LW RRTMG scheme	Iacono et al. (2008)
Shortwave radiation	SW RRTMG scheme	Iacono et al. (2008)
Time period	March-25th <u>25 March</u> - April-10th <u>10 April</u> , 2019	
Spatial resolution	9 × 9 km	
Vertical layers	35 levels	
CMAQ		
Chemical mechanism	CB05eh51_ae6_aq	Sarwar et al. (2015)
Emissions	EDGAR version 5.0	Crippa et al. (2020)
Boundary conditions	CAM-Chem (adjusted)	Buchholz et al. (2019)
Heterogeneous reactions	HOBr + ASEACAT = Br ₂ + H ₂ O + ASEACAT	Based on Mellberg (2014)
Initial conditions	Profile (build-in)	
Time period	March-28th <u>28 March</u> - April-6th <u>6 April</u> , 2019	

2.1.1 WRF

100 The WRF model version 3.9.1, developed by National Center for Atmospheric Research (NCAR) and National Oceanic and Atmospheric Administration (NOAA), was used to ~~capture~~ simulate the meteorological fields (Skamarock et al., 2008). The initial conditions and boundary conditions of WRF were given by GDAS/FNL (the Global Data Administration System / Final) re-analysis dataset (National Centers for Environmental Prediction et al., 2015), with a spatial resolution of $0.25^\circ \times 0.25^\circ$ and a temporal resolution of 6 h. The computational domain used in WRF and CMAQ is shown in Fig. 1(b), of which the center

105 is 70.0° N, 156.8° W. The spatial resolution was set to ~~9km~~ 9 km. Along the vertical direction, 35 layers were distributed. The time period of the WRF simulation ranges from ~~March-25th to April-10th~~ 25 March to 10 April, 2019. The detailed settings of the WRF model are given in Table 1.

2.1.2 CMAQ

In this study, a 3-D regional air quality model, CMAQ, developed by the United States Environmental Protection Agency (EPA), was used to capture the ODEs. CMAQ combines atmospheric science and air quality models together and uses multi-processor technology for three-dimensional simulations of ozone, ~~particulate matters~~ particulates and acid deposition (US EPA Office of Research and Development, 2020). In the present study, CMAQ versions 5.2.1 (US EPA Office of Research and Development, 2018) was used to capture the ~~variation~~ variations of ozone and other atmospheric constituents during ODEs. The equation denoting the change of each chemical species in CMAQ is shown below:

$$\frac{\partial c}{\partial t} = \text{Adv} + \text{Diff} + R_c + E_c + S_c. \quad (1)$$

In Eqn. (1), $\frac{\partial c}{\partial t}$ denotes the temporal change of ~~the~~ chemical species. The terms on the right hand side of Eqn. (1) represent advection, diffusion, chemical conversion of species c , emissions of species c , and loss of species c , respectively (US EPA Office of Research and Development, 2018). Eqn. (1) also covers processes elucidated by the process analysis method adopted in this study, which will be presented in a later context. The time period simulated in CMAQ ranges from ~~March 28th to April 6th~~ 28 March to 6 April, 2019. More details of the CMAQ configuration can be found in Table 1.

The chemical mechanism originally ~~instrumented~~ incorporated in CMAQ, CB05eh51_ae6_aq, was used in this study, which ~~considers~~ includes the halogen chemistry (Sarwar et al., 2015; Sherwen et al., 2016; Yarwood et al., 2012). A complete ~~listing~~ list of reactions in this mechanism can be found ~~in~~ on the website of CMAQ (EPA, 2023). However, the important heterogeneous reaction that determines the bromine explosion mentioned above is still lacking in this mechanism. Thus, we added one reaction into this mechanism:



In Reaction (R3), ASEACAT represents the number concentration of sea-salt aerosols in the model. Based on the study of Mellberg (2014), a reaction coefficient $k = 1.54 \times 10^{-14} \text{ molecules}^{-1} \cdot \text{cm}^3 \cdot \text{s}^{-1}$ was given to Reaction (R3) in the mechanism. This reaction coefficient used in the present study is ~~one order ten times~~ larger than that proposed by Mellberg (2014). It is because that in the study of Mellberg, bromine concentrations were reported to be underestimated by 5 to 10 times compared to observed values. Furthermore, only using this reaction coefficient can result in a reasonable simulation of ODEs in ~~the present study~~ our study. In order to clarify the role of this added heterogeneous reaction, we performed sensitivity tests by altering the rate coefficient of this reaction, which will be presented in Sect. 3.4 Sensitivity tests.

In addition, we found that in simulations, ozone and other species in the computational domain can be greatly affected by the implemented boundary conditions. Thus, we used a time-dependent boundary condition ~~adapted~~ taken from outputs of an earth system model, the Community Atmosphere Model with Chemistry (CAM-Chem) (Buchholz et al., 2019). However, the chemical mechanism used in CAM-Chem does not consider the influence of the bromine explosion mechanism (Emmons et al., 2020). Therefore, we modified the boundary ~~conditions~~ condition of ozone according to observations. ~~For the ozone in the boundary layer, if it is on the surface of~~ (Bottenheim and Chan, 2006). In the study of Bottenheim and Chan (2006), air with low ozone mole fractions was found to have passed over the Arctic Ocean. Moreover, they found that over the Beaufort

Sea and the Chukchi Sea, where the sea ice is frequently formed, the ozone value in the lower troposphere is normally in a range of 0-5.2 ppb. Thus, in the boundary condition of the model, when the air is in the boundary layer and over the sea ice, ~~ozone was set~~ we set the ozone value to 3 ppbv; ~~if it~~ ppb. Meanwhile, in the study of Bottenheim and Chan (2006), the ranges of ozone over the open sea and the coastal area were found to be 5.2-13.85 ppb and 5.2-24.45 ppb, respectively. Thus,
145 ~~in our model, if the air~~ is over the sea, ~~the boundary layer~~ ozone was set to 10 ppbv; ~~if it~~ ppb; and if the air is at a coastal area, ~~the boundary layer~~ ozone was set to 15 ppbv. ~~Furthermore, because the free atmospheric ozone can also~~ ppb. In addition, Bottenheim and Chan (2006) also suggested that the free tropospheric air can be remarkably affected by the bromine explosion ~~and the ODEs, ozone in the free troposphere in the implemented boundary condition,~~ and ODEs can also be influenced by the air transported from the free troposphere. Thus, in the boundary condition of the model, ozone in the free troposphere
150 was also reduced to half of the original value to consider the influence of the bromine explosion. ~~Due to the uncertainty in simulations caused by implementing this modified boundary condition, sensitivity tests were also performed by switching on/off this boundary condition in the CMAQ model, of which the results will be presented in Sect. 3.4.~~ The detailed settings of the boundary conditions can ~~also~~ be found in Section *Code and data availability*.

~~The emissions~~ Emissions used in CMAQ were generated by Sparse Matrix Operator Kernel Emissions (SMOKE) developed
155 by EPA (Baek and Seppanen, 2019). EDGAR (Emissions Database for Global Atmospheric Research) version 5.0 was implemented in SMOKE as the emission inventory (Crippa et al., 2018, 2020; Pesaresi et al., 2019; Monforti-Ferrario et al., 2019). A surf zone of 50 m was also set up in the present model, due to the existence of ocean in our computational domain. By doing that, more sea spray can be released from the surf zone.

Aside from studying the temporal ~~variation~~ variations of chemical species, we also used PA, i.e., process analysis (Gipson,
160 1999), to ~~quantitatively~~ estimate the contribution from each physical or chemical process to the ~~variation of a selected air constituent~~ variations of selected air constituents. PA is a module originally included in CMAQ. By performing PA, we were able to analyze the changes of ~~the~~ selected species and quantitatively assess the importance of influencing factors. Integrated Process Rate (IPR) and Integrated Reaction Rate (IRR) were calculated in the PA module. The former includes the net change of species ~~through~~ contributed by advection, diffusion, emissions, deposition, and the overall effect of chemical ~~process~~ processes.
165 The latter calculates the variation caused by each chemical reaction in the mechanism (Gipson, 1999).

2.2 ~~Observational Data~~ Measurements

2.2.1 ~~Ground-based observations~~

The observational data were obtained from the Global Monitoring Laboratory (GML, <https://gml.noaa.gov/aftp/data/barrow/>), which belongs to National Oceanic and Atmospheric Administration (NOAA). The observational data included surface ozone
170 (McClure-Begley et al., 2014) and meteorological parameters such as wind direction, wind speed at 10 m, pressure, temperature at 2 m and 10 m, and relative humidity (Mefford et al., 1996; Herbert et al., 1986a, b, 1990, 1994). In this study, we focused on the spring of 2019, of which the ~~observational data measurements~~ are shown in Fig. 2. We chose ~~March 25th to April 10th~~
~~March to 10 April~~, 2019 ~~for simulation~~ to simulate. In this time period, several complete ODEs, of which the minimal ozone is

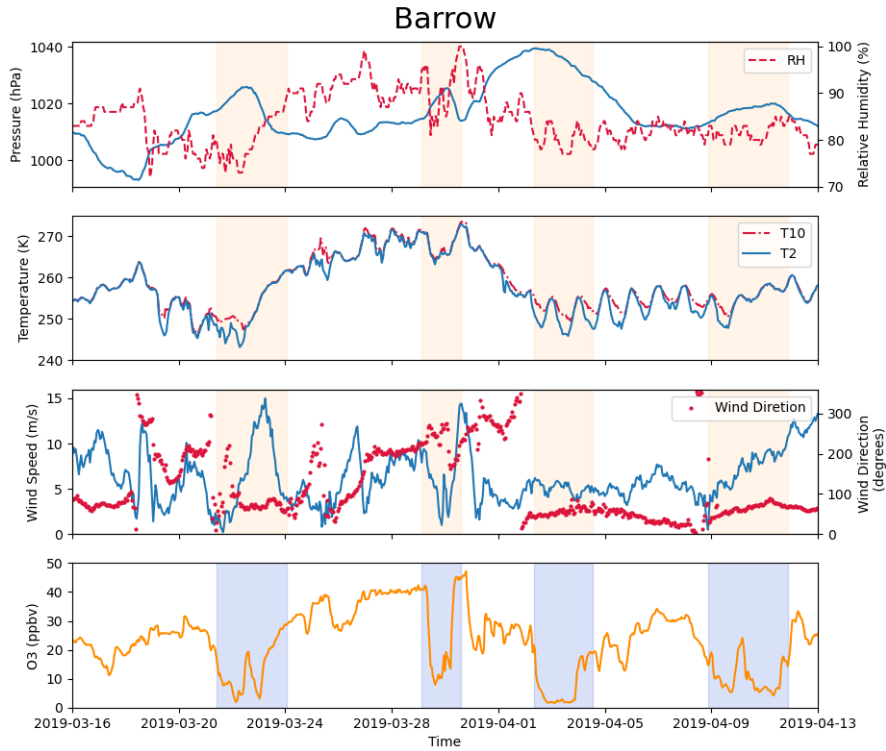


Figure 2. Measurements of pressure, relative humidity, temperature at 2 m and 10 m, wind direction, wind speed at 10 m and surface ozone at Barrow (now known as Utqiagvik) from 16 March to 13 April, 2019. The shaded areas denote the occurrence of complete ODEs, of which the minimal ozone is less than 10 ppb.

less than 10 ppb, are included (see the shaded areas in Fig. 2). Synoptic charts during this period with the surface analysis were also obtained from the Weather Prediction Center, shown in the supplements Fig. S1 in the Supplementary Information.

To validate the simulations, we used the Pearson correlation coefficient (R) and the root-mean-square error (RMSE) calculated as follows:

$$R = \frac{\sum_{i=1}^N (S_i - \bar{S})(O_i - \bar{O})}{\sqrt{\sum_{i=1}^N (S_i - \bar{S})^2 \sum_{i=1}^N (O_i - \bar{O})^2}}, \quad (2)$$

$$RMSE = \sqrt{\frac{\sum_{i=1}^N (S_i - O_i)^2}{N}}. \quad (3)$$

In Eqns. (2) and (3), S_i and O_i represent the simulated value and the observed value at the i th time point, respectively. N represents the total number of the time points. \bar{S} and \bar{O} stand for the time-averaged values during this time period, correspondingly. R ranges from -1 to 1. The closer the absolute value of R is to 1, the better simulations match the observa-

tional data. When the value of R is larger than 0.7, it indicates a very strong positive correlation. For RMSE, a smaller RMSE represents a less deviation between simulations and observations.

185 2.2.2 Satellite data

We also compared the tropospheric BrO column density simulated by the model with the satellite data. The simulated tropospheric BrO column density was calculated as follows:

$$\rho_{\text{BrO}} = \int_0^{\text{Tropopause}} \frac{p \cdot c_{\text{BrO}}}{R^* \cdot T} dh. \quad (4)$$

190 In Eqn. (4), ρ_{BrO} denotes the column density of the tropospheric BrO (unit: $\text{nmol} \cdot \text{m}^{-2}$). The right hand side of Eqn. (4) represents an integration of the BrO concentration from the ground to the top of the troposphere, in which p , c_{BrO} , R^* , T and h denote the pressure at this height (unit: Pa), the BrO concentration (unit: ppb), the molar gas constant (unit: $\text{J} \cdot \text{K}^{-1} \cdot \text{mol}^{-1}$), the temperature (unit: K) and the height (unit: m), respectively. The satellite observations of the tropospheric BrO column density were obtained from EUMETSAT SAF on Atmospheric Composition Monitoring (AC SAF, 2022).

The detailed simulation results are shown in the following section.

195 3 Results and Discussions

In this section, we will demonstrate the reliability of the simulations first, and then discuss the simulated ODEs in detail. Later, uncertainties in our simulations are illustrated through sensitivity tests, by changing the rate of the heterogeneous reaction and switching on/off the implemented boundary condition. At last, a comprehensive process analysis of each ODE was conducted. All geographic names mentioned in the following content can be found in Fig. 1(a).

200 3.1 Validation of the simulations

The temporal ~~variation of the meteorological field~~ (variations of meteorological parameters including temperature, horizontal components of the wind speed, and pressure ~~)~~ in Barrow simulated by WRF was/were compared with the observational data, shown in Fig. 3. It can be seen that during this period, the pressure of Barrow (71.3230° N, 156.6114° W) is generally in a trend of first increasing and then decreasing, with an obvious abrupt decrease from 30 to 31 March ~~30th to 31st~~ (Fig. 3a). This significant decline of the pressure corresponds to a remarkable ~~drop change~~ drop change in temperature and ~~a rapid change in the~~ horizontal components of wind speed, U and V (see Fig. 3c and d). All Values of all the statistical parameters can be found in Table S1 of the supplementary material. The correlation coefficients (R) of pressure, temperature, U and V between simulations and observations are 0.991, 0.920, 0.920, 0.881 and 0.897, respectively. These correlation coefficients are all very close to 1.0, indicating a high agreement between observations and simulations. The RMSEs of pressure, temperature, U and V are 3.081 hPa, 3.784 K, 210 2.153 $\text{m/s} \cdot \text{s}^{-1}$ and 2.282 $\text{m/s} \cdot \text{s}^{-1}$, respectively. They also denote small deviations between observations and simulations. Thus,

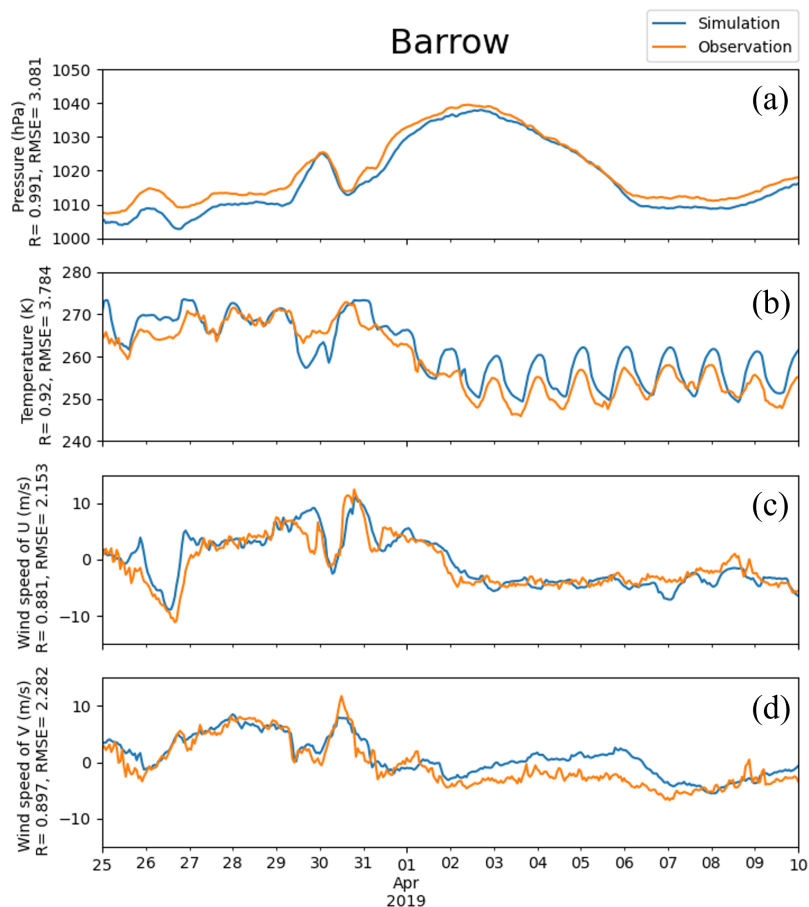


Figure 3. Pressure, temperature, horizontal components of 10-m wind (U and V) obtained from simulations and observations in Barrow from 25 March to 10 April, 2019. The correlation coefficient R and the root-mean-square error RMSE were also presented in the vertical axis.

we can conclude that the simulated meteorological field is accurate, so that it can be used to drive the chemical simulations of CMAQ during this time period.

The temporal variation of the surface ozone in-at Barrow simulated by CMAQ was then compared with the observational data, shown in Fig. 4. During this period, the surface ozone at Barrow changed dramatically, and three ODEs were observed.

- 215
1. On March-29th29 March, from 07 to 16 UTC, ozone declined from 41.6 ppb to 9.0 ppb, then on March-30th30 March from 05 to 10 UTC, ozone recovered from 13.6 ppb to 45.2 ppb.
 2. Later, from 19 UTC on March-30th30 March to 04 UTC on March-31st31 March, a partial ODE occurred. The surface ozone declined from 47.2 ppb to 19.9 ppb. Then at 10 UTC on March-31st31 March, ozone recovered from 18.7 ppb to 32.6 ppb within three hours.

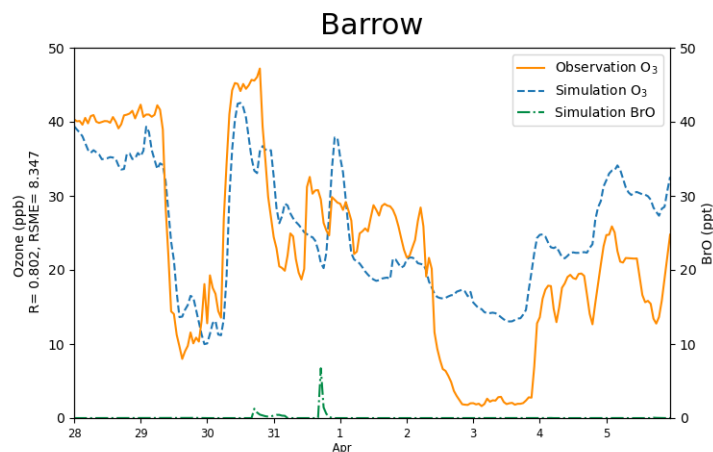


Figure 4. The surface ozone (ppb) obtained from simulations and observations together with the simulated BrO in at Barrow from 28 March 28th to 5 April 5th, 2019. The correlation coefficient R and the root-mean-square error RMSE were also presented in the vertical axis.

220 3. A complete ODE occurred on April 2nd 2 April. From 05 UTC to 22 UTC, ozone decreased from 28.4 ppb to 1.8 ppb. After a whole day of low values, ozone resumed from 2.8 ppb to 17.9 ppb.

The correlation coefficient and the root-mean-square RMSE (RMSE) of the surface ozone between the simulations and the observations are 0.793 and 8.407 0.802 and 8.347 ppb, respectively. The trend Thus, the variation tendency of the surface ozone was also well generally reproduced (see Fig. 4), including those dramatic changes discussed above. In particular, ODEs on March 29th, March 31st, and April 2nd were captured, not only the start of the ODEs, but also the recovery of them. It enables us for the subsequent analysis. It the ODEs were captured in simulations. However, it should be noted that although our simulations fit the observations well, there still exist a fraction of mismatches between simulations and observations. For example, for the complete ODE on 2 April, the model overestimated the surface ozone by approximately 10 ppb. After performing many sensitivity tests (shown in Sect. 3.4), we found this ODE to be greatly contributed by a transport of low-ozone air from the Arctic Ocean which is located to the north of Barrow. As a result, the simulation of this ODE is heavily influenced by the implemented boundary condition of the model. Although we have modified the boundary condition based on observations, which has been described in Sect. 2.1.2, the simulation results still show some deviations from the observations, possibly indicating that improvements of the implemented boundary condition and the adopted chemical mechanism are still needed. Moreover, for the ODE on 29 March, possibly due to the uncertainty in boundary conditions. For example, due to the particularity of the ODE on from the satellite measurements (Fig. S2 in the Supplementary Information), we found a high BrO level in regions of the Chukchi Sea and the Chukotka Peninsula (66.8° N, 176.6° W) at 22:44:15 UTC on 28 March 29th, ozone over the Chukotka Peninsula in the implemented boundary conditions was adjusted 2019 (see Fig. S2a). These high BrO regions were also found in satellite measurements at the next time point (see Fig. S2b). Because the elevated BrO may reflect a depletion of ozone in these regions, we also modified the boundary condition of the model by reducing the ozone over the

225

230

235

240 Chukotka Peninsula to 40% of its original value during this time. Simulation results without this adjustment-modification are shown in Fig. S1-S3 in the supplement. It can be seen that without this adjustment-modification, the simulated ozone on March 29th-29 March would be largely different from the observations observations. More results about the uncertainties caused by the implemented boundary condition will be presented and discussed in Sect. 3.4.

245 We also used satellite data to validate our BrO simulations. However, only a qualitative agreement between the simulated BrO and the observations can be achieved. For example, in simulations and observations, regions with high BrO column density were both found to the northwest of Barrow on 30 March (see Fig. S4 in the Supplementary Information). Besides, in simulations, the maximum of BrO was found to be approximately 2000 nmol/m², which is similar to the peak value in satellite observations. For a better comparison, improvements of the model such as adding the iodine chemistry and more heterogeneous reactions need to be made, which is attributed to a future work.

250 3.2 Comprehensive analysis of each ODE

In the previous section, we mentioned that during this period, the pressure of Barrow is generally in a trend of first increasing and then decreasing, with an obvious abrupt decrease from March 30th to 31st (30 to 31 March (see Fig. 3a). These meteorological changes at Barrow mainly resulted from two weather conditions, a cyclone and an anti-cyclone, respectively. Under these circumstances, three ODEs occurred. From our simulations, we found that the ODE occurring on March 29th in on 29
255 March at Barrow mainly formed by a transport of low-ozone air masses to the west of the Chukchi Sea (71.7° N, 169.9° W), so that the simulation of this ODE is heavily determined by the applied boundary conditions of the model. Thus, we will not investigate it deeper in this study. The following two ODEs, occurring on March 31st-31 March (named as ODE1) and April 2nd-2 April (named as ODE2), will be analyzed in detail below.

3.2.1 ODE1 (on 31 March~~31st~~)

260 The spatial distribution-distributions of the surface temperature and the pressure from March 30th to March 31st was 30 March to 31 March are shown in Fig. 5. Globally, during this period, the Arctic Ocean (79.0° N, 156.9° W) was dominated by the Arctic vortex, of which the center pressure was low (1002 hPa) and the center temperature was less than -24°C. In contrast, the mainland of Alaska was covered by a uniform pressure field. Figure 5(a) shows that at UTC 00 on March 30th UTC on 30 March, the gradient of the air temperature on the Beaufort Sea (73.7° N, 146.6° W) was very large. This large temperature
265 gradient was formed due to the passing by of a cold front in this area (see Fig. S2b in the supplements S1b in the Supplementary Information denoting the weather patterns). At the same time, the temperature field around the Chukotka Peninsula became twisted (see also deformed (see Fig. 5a). A low-pressure system (i.e., a cyclone) was also formed over the Chukchi Sea. Then, the low-pressure system developed rapidly and moved northeastward. Meanwhile, the meteorological field-fields around the cyclone was-were distorted accordingly, especially the temperature. At 12 UTC on March 30th-30 March shown in Fig. 5(b),
270 the center of the low-pressure system reached 1008 hPa. This low pressure system also generated a cold front on the left and a stationary front on the right (see Fig. S2d in the supplements S1d in the Supplementary Information), leading to a strong temperature gradient around this low pressure. Then, at 00 UTC on March 31st-31 March (Fig. 5c), the low-pressure system

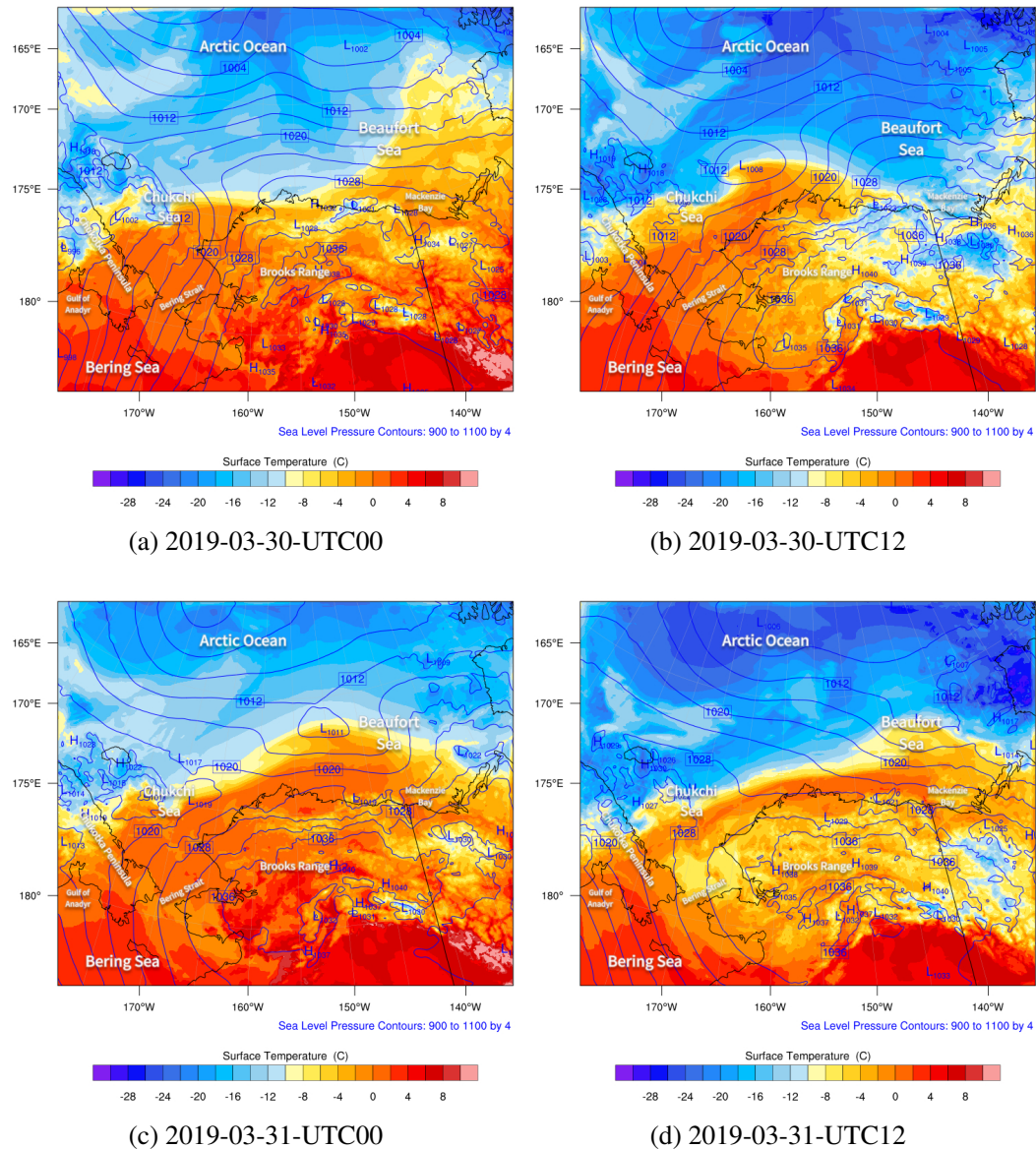


Figure 5. The spatial ~~distribution~~distributions of the sea level pressure (hPa, contour lines) and surface temperature ($^{\circ}\text{C}$, contour fills) simulated by WRF from 30 March ~~30th~~30th to 31 March~~31st~~31st, 2019.

275 moved to the north of Barrow, and its center pressure increased to 1011 hPa, which means the weakening of the low-pressure system. Within a couple of hours (see Fig. 5d), the cyclone continued moving eastward, but a front remained over the sea.

For the meteorological field with a finer time interval, please refer to Fig. ~~S3 in the supplements~~S5 in the Supplementary Information.

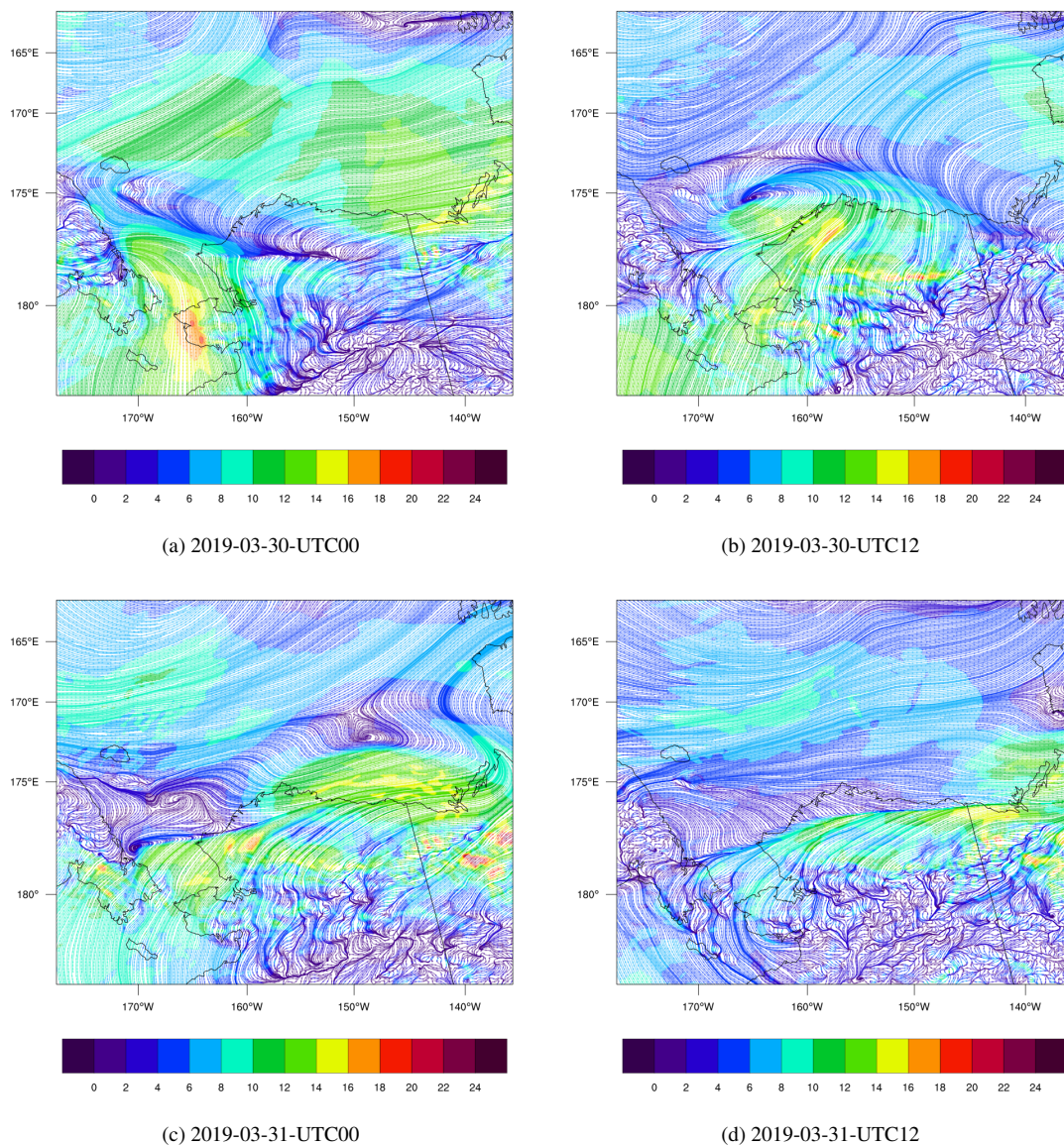


Figure 6. The spatial distribution of surface wind ($\text{m}/\text{sm} \cdot \text{s}^{-1}$) and the streamline simulated by WRF from March 30th 30 March to 31 March 31st, 2019.

The spatial distribution of the surface wind from March 30th to March 31st 30 March to 31 March is shown in Fig. 6. Figure 6(a) shows that at 00 UTC on March 30th 30 March, the wind speed over the Bering Strait (66.0° N, 168.9° W) was very large, of which the maximum reached 18 $\text{m}/\text{sm} \cdot \text{s}^{-1}$. With such a high wind speed, sea-salt aerosols can be rapidly released into the atmosphere (see shown in Fig. S4b in the supplements S6b in the Supplementary Information). The liberation of sea-salt aerosols causes a release of is able to release the reactive bromine into the atmosphere, which can deplete the surface ozone.

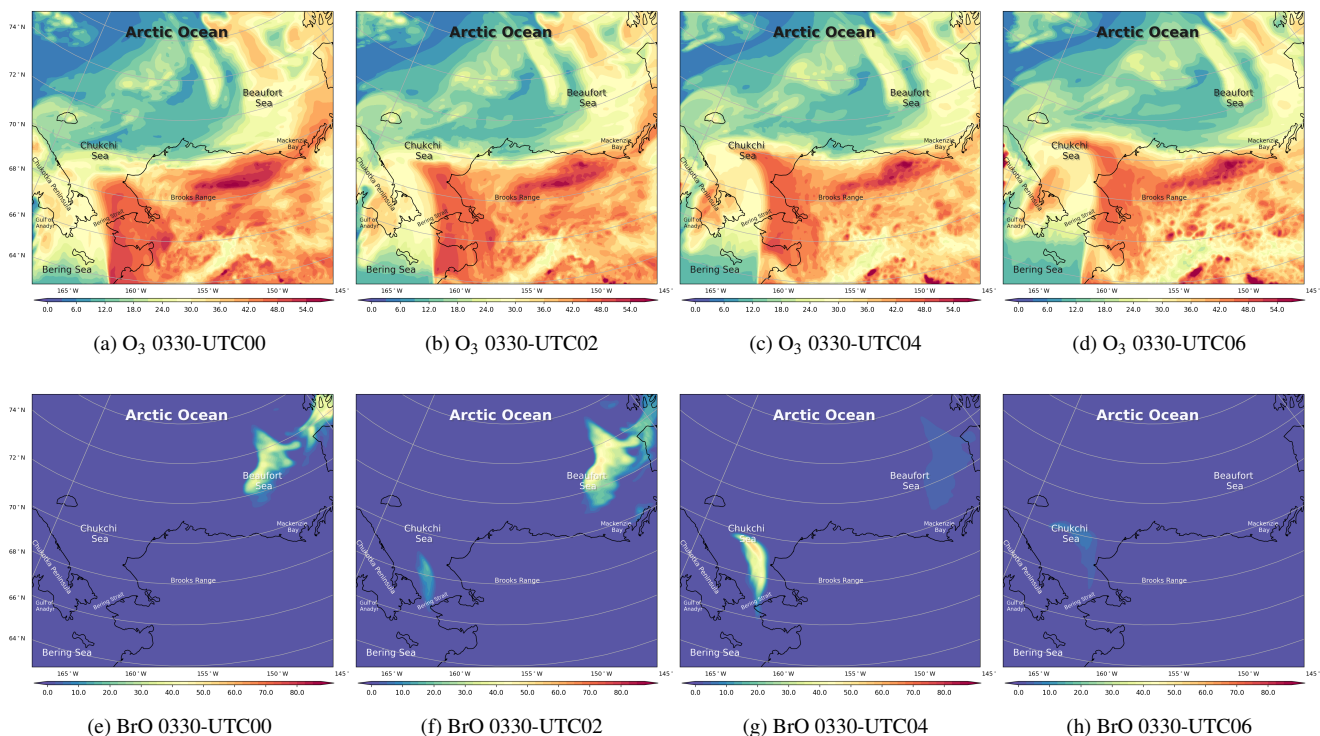


Figure 7. The spatial distribution of the surface ozone (ppb) and BrO (ppt) simulated by CMAQ on 30 March 30th, 2019.

At UTC12 on March 30th-12 UTC on 30 March shown in Fig. 6(b), the wind was cyclonic over the Chukchi Sea and the wind speed was quite large between the two fronts mentioned above. Then, in Fig. 6(c), at UTC00 on March 31st-UTC on 31 March the cyclone moved eastward and the wind speed decreased. After 12 hours (see Fig. 6d), the wind speed in this area was low. The cyclone moved to the south of the Banks Island -(73.48° N, 121.8° W), which indicates the end of this process. For the surface wind with a finer time interval, please refer to Fig. S5 in the supplements S7 in the Supplementary Information. This process is similar to the “bromine cyclone transport event” described by Blechschmidt et al. (2016), but the scale of the process discussed in this study is smaller than that of Blechschmidt et al. (2016).

The spatiotemporal distribution distributions of the simulated ozone and BrO on March 30th is 30 March are shown in Fig. 7. We mentioned above that under the high-wind-speed conditions, a large amount of sea-salt aerosols can be carried into the atmosphere, as early as March 29th 29 March (see Fig. S4a in the supplements S6a in the Supplementary Information). However, changes in ozone and BrO were not revealed until 00 UTC on March 30th 30 March, which means that the response of the chemical field to the change in meteorology is retarded delayed. Figure 7(a) shows that, over the Arctic Ocean, the surface ozone was at a low level at UTC00 on March 30th UTC on 30 March. In contrast, over the mainland of Alaska, the surface ozone remained at a background level. BrO-BrO is an indicator of ODEs because it increases rapidly during the depletion of ozone. Thus, when ozone at the Gulf of Anadyr and the north of Banks Island near the Chukchi Sea and the Beaufort Sea

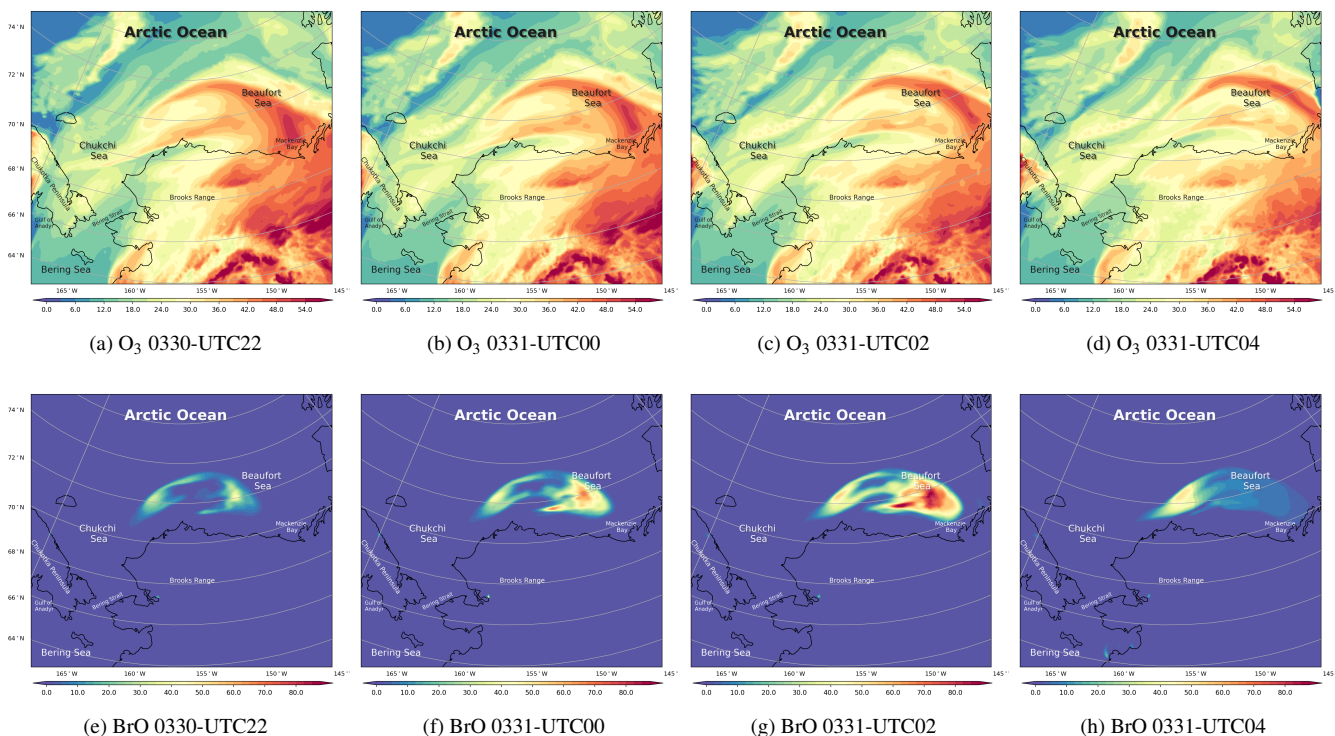


Figure 8. The spatial distribution of the surface ozone (ppb) and BrO (ppt) simulated by CMAQ from March 30th 30 to 31st 31 March.

began to decrease (Fig. 7a and b), the surface BrO started to generate shown in (Fig. 7(e and f)). In the next 4 hours, the surface ozone at the Bering Strait continued its depletion near the Chukchi Sea declined continuously as shown in Fig. 7(c), leading to a strong ozone gradient there. Meanwhile, BrO at this place is explosively generated, shown in Fig. 7(f) and (g).
 300 The maximum of BrO over the Bering Strait was larger than 10060 ppt, of which the high value areas were consistent with the region regions abundant in sea-salt aerosols (Fig. S4 in the supplements S6 in the Supplementary Information). Then, under the control of the strong wind, the air mass with depleted ozone and abundant bromine moved northeastward. Moreover, because of the cyclonic wind discussed above, the air mass containing the depleted ozone and abundant bromine was twisted (see Fig-7e and g). At UTC deformed. At 06 on March 30th, the sunset occurred UTC on 30 March, the sun was setting. The low-ozone
 305 area stopped expanding. The high-BrO area also disappeared due to the absent of the photolysis of Br₂ photolysis.

The spatiotemporal distribution distributions of the surface ozone and BrO from March 30th to 31st was BrO from 30 March to 31 March were also shown in Fig. 8. At UTC22 on March 30th shown in 22 UTC on 30 March (Fig. 8(a)), the sun rose again and the photochemistry started. It can be seen in Fig. 8(a) and (b) that the chemical field of ozone was twisted deformed strongly, under the eyclonie wind on control of the cyclonic wind to the north of Barrow. Meanwhile, the reactive
 310 bromine returned to the atmosphere by due to the bromine explosion mechanism shown in (Fig. 8(e)). Then at 00 and 02 UTC on March 31st 31 March (see Fig. 8f and g), BrO increased explosively over time. Within 4 hours, the mixing ratio of BrO

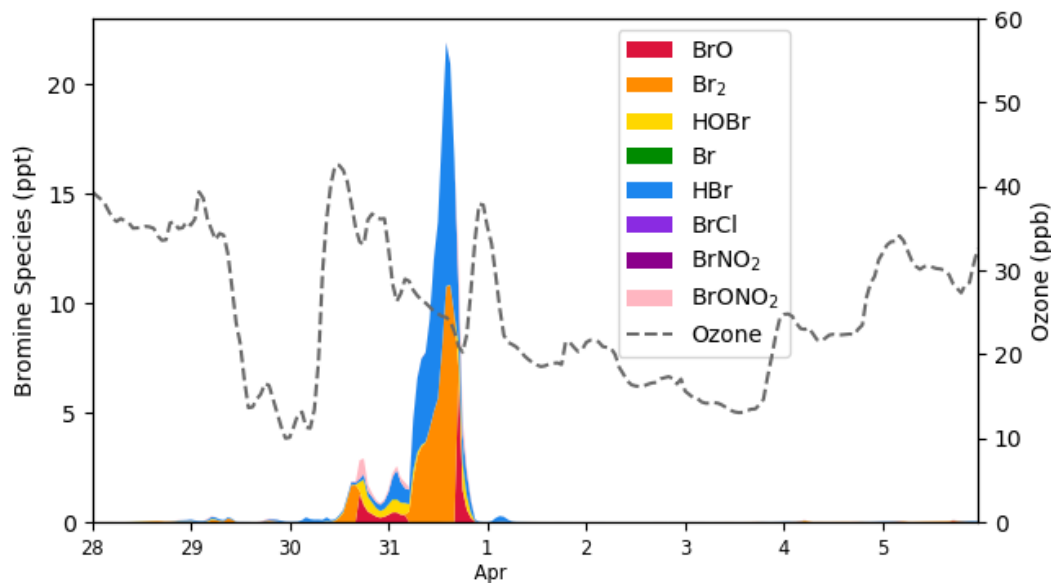


Figure 9. The temporal behavior of bromine species (ppt) and ozone (ppb) simulated by CMAQ at Barrow from 28 March to 6 April, 2019.

surface BrO reached a maximum larger than 100 ppt over the Beaufort Sea, which is consistent with the spatial distribution of sea-salt aerosols (see Fig. S4f-S6f and g in the supplementsSupplementary Information). Correspondingly, the surface ozone decreased continuously (see Fig. 8c), but the decrease was slightly behind the increase of BrO. The mixing ratio of the surface ozone had been as low as 10 ppb over the north of the Mackenzie Bay. At 04 UTC on March 31st 31 March (see Fig. 8h), the source of BrO was again cut off due to the sunset. The amount of BrO in areas where the sunset occurred was much In places where the sun set, the level of BrO was significantly lower than that in which the sunset did not occur places where the sun did not set. In contrast, the change in the surface ozone is a little bit retarded. The minimum of the surface ozone at UTC02 on March 31st (~5 ppb over the north Mackenzie Bay, see Fig. 8d) was even lower than that at previous time points, and the area of the low ozone was also larger, slightly delayed.

In general, during the time period between March 29th and March 31st, local chemical processes led to the complete ODE 29 March and 31 March, the local chemical process, i.e., bromine chemistry, contributed to the partial ODE and the increase of bromine over the Beaufort Sea. The center of this ODE was mainly over the north of the Maekenzie Bay, with a because of the high wind condition and the release of sea-salt aerosols. A maximum of BrO larger than 80 ppt and a minimum of the surface ozone smaller than 15 ppb was found over the sea during this ODE. In contrast, the BrO level observed at Barrow during this time was less than 10 ppt. Thus, we suggested that BrO in the center of the ODE was much larger than that observed at Barrow. Hence, more observations of ozone and bromine over the ocean in the Arctic are required to better understand the properties of ODEs and the bromine explosion mechanism.

The temporal profiles of bromine species and ozone in Barrow at Barrow in simulations are shown in Fig. 9. We can see that the bromine species especially Br₂ began to increase on March 30th 30 March. After the sunrise, Br₂ photolyzed immediately,

releasing two bromine atoms. These bromine atoms then ~~consumed~~ react with the surface ozone, ~~forming and form~~ BrO. Moreover, bromine is continuously released into the atmosphere due to the bromine explosion mechanism. As a result, under this ~~circumstances~~ circumstance, ozone began to decrease while BrO burst into the atmosphere. ~~On March 31st, the maximum of BrO in Barrow reached 21.25 ppt in the daytime.~~ Meanwhile, as BrO also reacts with HO₂, ~~forming and forms~~ HOBr, the amount of HOBr also increased during this time. When the ~~sunset occurred~~ sun set, due to the absent of the Br₂ photolysis, BrO declined while HBr and Br₂ accumulated rapidly. The concentration of HBr and Br₂ peaked at ~~44.7~~ 10.8 ppt and ~~28.5~~ 11.1 ppt, respectively. Ozone remained at a relatively low level at this time. Then, ~~when the sun rose again,~~ Br₂ photolyzed rapidly and BrO was formed again, reaching a peak of 6.64 ppt in the daytime. Afterwards, the air mass ~~in at~~ in at Barrow was carried eastward, the bromine species ~~in at~~ in at Barrow thus declined and the ozone recovered.

340 3.2.2 ODE2 (on 2 April)

Regarding the ODE ~~occurring on April 2nd~~ on 2 April (ODE2), we first focused on the weather conditions. During this time, Barrow and its surrounding areas were occupied by a high-pressure system with a cold center from ~~April 2nd to April 4th~~ 2 April to 4 April (see Fig. ~~S6 in the supplements~~ S8 in the Supplementary Information denoting the surface temperature and pressure). Under the control of this high-pressure system, a stable stratification with light anticyclonic winds (less than ~~5 m/s~~ 5 m/s) was formed in this area. A clear sky, which is a typical weather condition during ODEs (Rancher and Kritz, 1980; Simpson et al., 2007; Anderson and Neff, 2008; Bottenheim et al., 2009; Boylan et al., 2014; Swanson et al., 2020), was also observed. After that, the center of the anticyclone moved slowly southeastward (see Fig. ~~S7 in the supplements~~ S9 in the Supplementary Information for the surface wind fields).

Under this circumstance, ODEs occurred over the Beaufort Sea and Barrow (see Fig. 10). On ~~April 2nd~~ 2 April, due to the existence of the high-pressure system over the Arctic Ocean (see Fig. 10a), Barrow and its surrounding ~~area~~ areas were controlled by a northerly wind, so that air masses with low ozone from the Arctic Ocean were transported to Barrow. The situation ~~of with~~ a low-level surface ozone in at Barrow lasted for about one day (Fig. 10b and c). ~~Bottenheim and Chan (2006)~~ In the study of Bottenheim and Chan (2006), they also found that under the condition of a strong, stable stratification in the Arctic, it may take more time for the surface ozone recovering from the depleted status, so that the air parcel with depleted ozone can travel a long distance such as from the Arctic Ocean to Barrow. Then, the surface ozone of Barrow recovered to the background level, shown in Fig. 10(d). ~~This ozone recovery was~~ It should be noted that there exist some inconsistencies between ODE2 simulations and observations. Following many sensitivity tests and the process analysis, which will be presented in Sections 3.4 and 3.5, we concluded that this ODE detected at Barrow was mainly caused by a transport of low-ozone air from the Arctic Ocean, of which the simulation is heavily affected by the implemented boundary condition. In contrast, the recovery of this ODE was mainly caused by a vertical transport of ozone-rich air from the free atmosphere into the boundary layer, which will be shown and discussed in a later context. For the variation of the surface ozone with a finer time interval, please refer to Fig. ~~S8 in the supplement~~ S10 in the Supplementary Information.

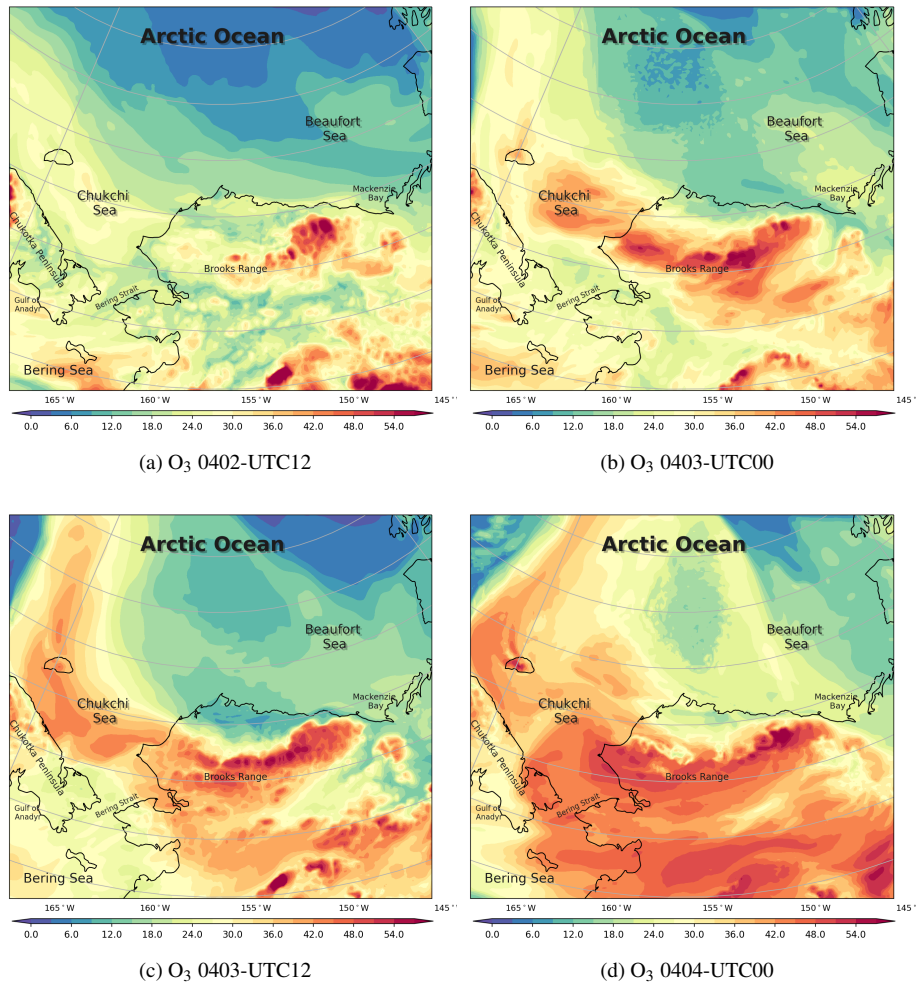


Figure 10. The temporal behavior spatial distribution of bromine species (ppt) and the surface ozone (ppb) simulated by CMAQ in Barrow from March 28th 2 to 4 April 6th, 2019.

3.3 Vertical characteristics

The vertical profiles of ozone, BrO and the vertical wind speed, w , at Barrow below the height of 1000 m are shown in Fig. 11. As described above, during ODE1, a cyclone is formed over the Chukchi Sea and moved northeastward. Thus, at this time stage (on March 30th 30 March), the atmospheric activity is intense, and the boundary layer height in Barrow reached 1000 m (see Fig. 11a and b), significantly higher than the typical boundary layer height in Arctic, 100-500 m (Stull, 1988). Meanwhile, the vertical wind speed, w , changed dramatically. The vertical wind speed w was negative on the former half-day of March 30th 30 March (see Fig. 11c). Then on the latter half-day, w turned into positive. It denotes a vigorous turbulence in the boundary layer, so that BrO can be rapidly mixed aloft (see Fig. 11b). On March 31st 31 March, w was mostly positive within the whole

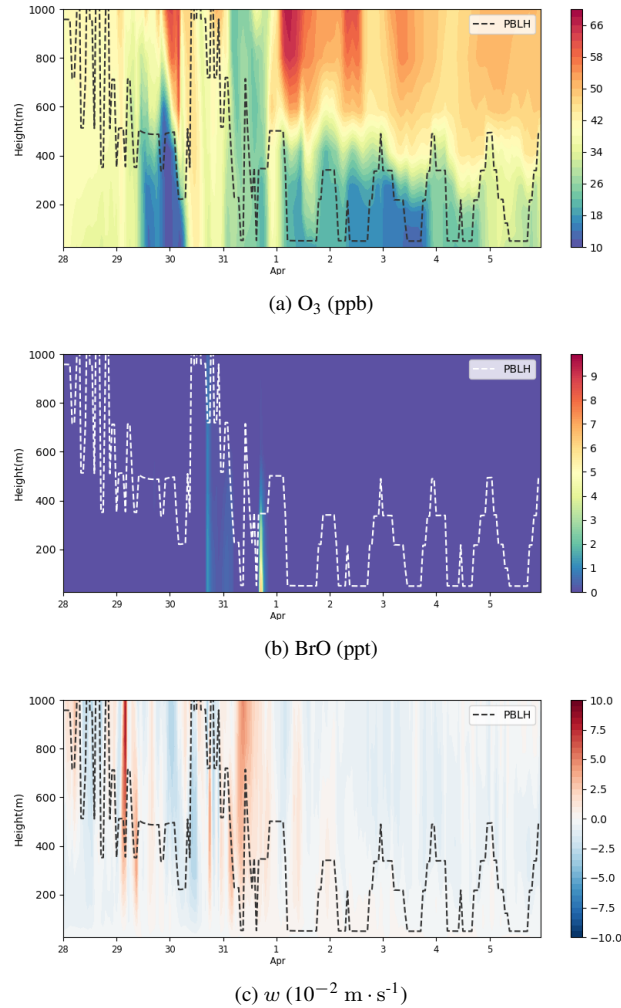


Figure 11. Vertical profiles of ozone (ppb), BrO (ppt) and vertical wind speed w (10^{-2} m/s) from 28 March 28th to 6 April 6th, 2019 in Barrow, in which the dotted line represents the local planetary boundary layer height (PBLH). A positive w represents an ascending tendency of air parcels while a negative w denotes a descending tendency of air parcels.

1000 m height. BrO was thus carried outside the boundary layer. It led to the occurrence of the partial ODE1 ubiquitously below the height of 1000 m. Therefore, at this time, the depletion of ozone is not limited within the boundary layer, and the ozone in the free atmosphere can also be influenced.

With respect to ODE2 during April 2nd-3rd 2-3 April, from the discussions above, Barrow and its surrounding areas were occupied by a high-pressure system. The boundary layer height in-at Barrow during this time was lower than that in March, and shows a distinct diurnal variation (see Fig. 11a). Moreover, ozone shows a strong concentration gradient, especially around the top of the boundary layer (see Fig. 11a). The-This strong concentration gradient was induced-maintained by the weak vertical diffusion under the stable stratification. In the study of Bottenheim and Chan (2006), they suggested that the stable

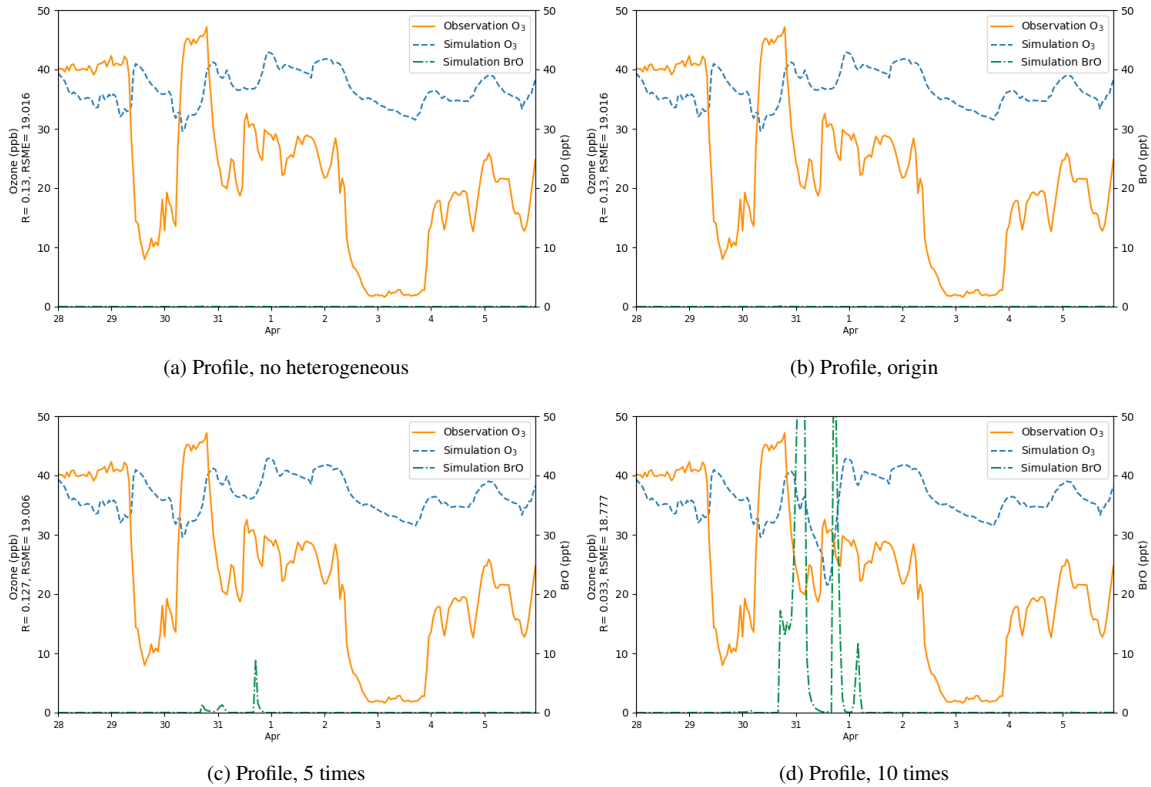


Figure 12. Surface ozone (ppb) and BrO (ppt) at Barrow from 28 March to 5 April, 2019, obtained from CMAQ simulations using different heterogeneous reaction rates and the default boundary condition, i.e., a static ozone profile. The correlation coefficient R and the root-mean-square error RMSE were also presented in the vertical axis.

stratification would inhibit the recovery of the ozone-lacking low-ozone status, which corresponded to the case of ODE2. At the end of ODE2, as shown in Fig. 11(c), the vertical wind speed was small but negative within these days. As time went by, ozone in the free troposphere was eventually mixed into the boundary layer, and the gradient of ozone is weakened, which represented was weakened, denoting the end of ODE2.

3.4 Sensitivity tests

Because the present simulations can be greatly affected by the rate of the heterogeneous reaction and the implemented boundary conditions (BC), we conducted a series of sensitivity tests and then analyzed the uncertainties induced by these two factors.

Results of the sensitivity tests in which the heterogeneous reaction rate was altered are shown in Fig. 12. In this series of sensitivity tests, we used the default BC of ozone in CMAQ. This default BC in CMAQ is generated by a static profile, which represents annual average concentrations over the Pacific for the year 2016. This BC reflects conditions in a remote marine environment. From Fig. 12(a), we found that with the default BC but without the heterogeneous reaction for the

Table 2. Values of the Pearson correlation coefficient (R) and the root-mean-square error (RMSE, unit: ppb) for the simulated surface ozone at Barrow under different conditions (the heterogeneous reaction rate and boundary conditions). The rate constant of the heterogeneous reaction suggested by Mellberg (2014) was multiplied by 0.0, 1.0, 5.0 and 10.0 and tested in different simulations. In addition, different boundary conditions (default BC in CMAQ, original CAM-Chem outputs, reduced CAM-Chem outputs but without the modification over the Chukotka Peninsula, reduced and modified CAM-Chem outputs) were also tested.

Rate \ BC	Default	CAM-Chem	CAM-Chem (reduced)	CAM-Chem (reduced & modified)
	(R, RMSE)	(R, RMSE)	(R, RMSE)	(R, RMSE)
0	0.130, 19.015			0.803, 8.339
1	0.130, 19.016			0.803, 8.339
5	0.127, 19.006			0.803, 8.339
10	0.033, 18.777	-0.398, 30.185	0.653, 10.223	0.802, 8.347

390 bromine explosion, the simulated ozone did not show any obvious depletion and the level of BrO was close to zero. Then we added the heterogeneous reaction (R3) responsible for the bromine explosion into the mechanism, with the reaction rate suggested by Mellberg (2014) (Fig. 12b), but found the changes in ozone and BrO negligible. Thus, we continued to enlarge the heterogeneous reaction rate. In Fig. 12(c), the reaction rate was 5 times larger than that suggested by Mellberg (2014). In this simulation, we found the BrO level at Barrow elevated, to a value range of 0-10 ppt. However, ozone did not show any remarkable change and the simulated value was still higher than the observations. In Fig. 12(d), we enlarged the heterogeneous reaction rate to a value that is 10 times of that suggested by Mellberg (2014), and we found the ozone during the time period of ODE1 (i.e., 31 March) decreasing to a level similar to observations. Moreover, BrO was also substantially elevated, with a peak higher than 50 ppt. However, ozone concentrations in other time periods were still not significantly influenced by the change of the reaction rate.

400 The statistical parameters for the simulated surface ozone at Barrow using different heterogeneous reaction rates are listed in Tab. 2. We can see that when the default static BC was used, the correlation coefficients were all close to 0.1. Furthermore, the RMSEs were also large. We also performed a simulation using a reaction rate that is 15 times of the rate proposed by Mellberg (2014), and the simulation results even show a negative correlation with the observations. Thus, from this series of sensitivity tests, we concluded that the heterogeneous reaction is only able to affect the simulated ozone and BrO during the time period of ODE1 (i.e., 31 March). For other time periods, other factors such as the implemented boundary condition (BC) might play important roles.

410 Then we tested different boundary conditions in simulations (Fig. 13). We first replaced the default BC with the outputs of the CAM-Chem model (Fig. 13a), but found the simulated ozone significantly higher than the observed values. As shown in Tab. 2, the correlation coefficient for this simulation is negative and the RMSE reaches 30.185 ppb. The reason for this large deviation might be the BC of ozone adopted from the CAM-Chem model does not take the influence of the bromine chemistry into account. Thus, we modified the outputs of the CAM-Chem model based on observations (Bottenheim and Chan, 2006).

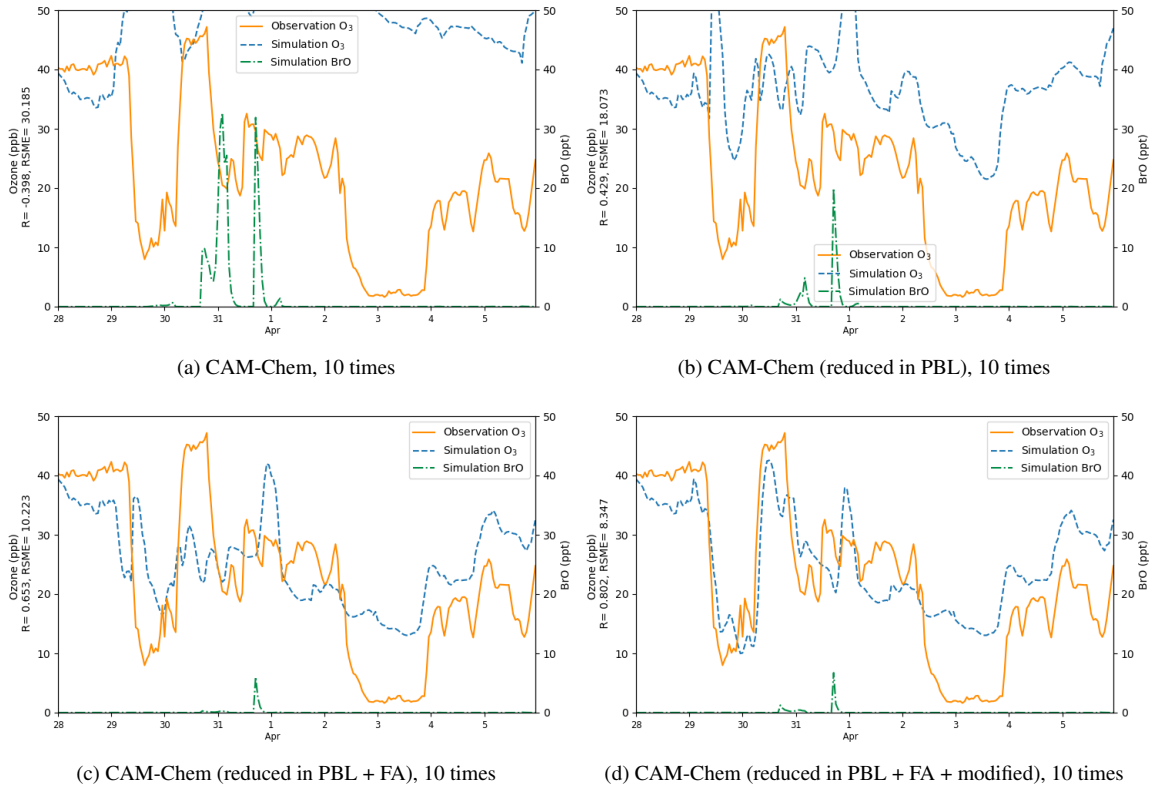


Figure 13. Surface ozone (ppb) obtained from simulations and observations together with the simulated BrO at Barrow from 28 March to 5 April, 2019. The correlation coefficient R and the root-mean-square error RMSE were also presented in the vertical axis. Simulations were performed using different boundary conditions: (a) time-dependent boundary conditions adopted from the outputs of CAM-Chem, (b) outputs of CAM-Chem with a reduction of ozone in the PBL, (c) outputs of CAM-Chem with a reduction of ozone in the PBL and the free atmosphere, (d) outputs of CAM-Chem with a reduction of ozone in the PBL and the free atmosphere as well as a modification of ozone over the Chukotka Peninsula.

by reducing the ozone in the PBL in the BC according to types of the underlying surfaces. Figure 13(b) shows that after this modification, compared with the previous simulation, the simulated ozone is lower during the whole time period, and the RMSE also decreases. It means that the BC of the model can substantially affect the simulation of ODEs at Barrow. However, the difference between the simulation results and the observations is still moderate. Then we discovered that the ODEs cannot only be affected by the air in the PBL, but also the air in the free atmosphere. Moreover, ozone in the free atmosphere can also be influenced by the bromine explosion (Bottenheim and Chan, 2006). Thus, we continued to reduce the free atmospheric ozone in the BC of the model (see Fig. 13c). It was found that the simulated ozone becomes lower than the previous simulation, denoting that the air transported from the free atmosphere also contributed to the ozone decline observed at Barrow. At last, we found that the ozone value over the Chukotka Peninsula in the BC of the model may exert a significant impact on the ODE on 29 March. Therefore, we modified the ozone over the Chukotka Peninsula in the BC of the model (see Fig. 13d). As a result,

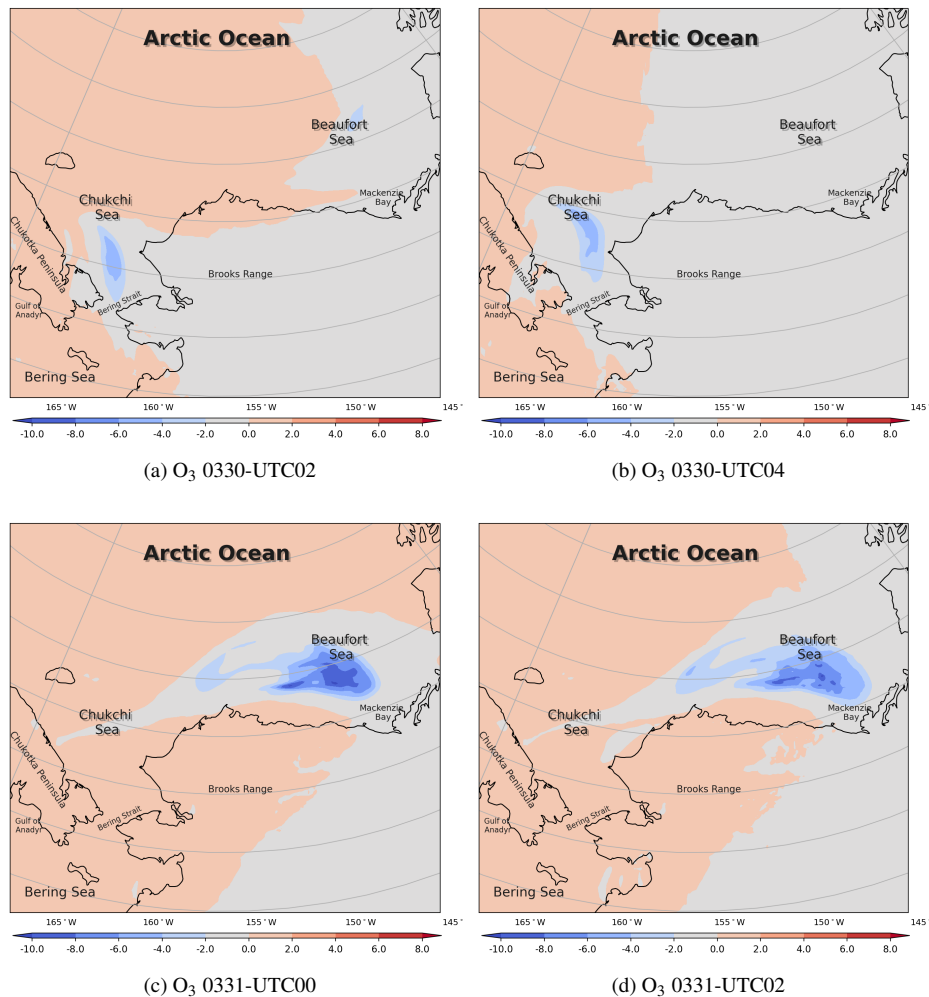


Figure 14. The change of surface ozone (ppb) caused by local chemistry, *i.e.*, bromine chemistry, from 30 March 30th to 31 March 31st, 2019. The positive value represents a chemical production of ozone, while the negative value represents a chemical consumption of ozone.

the simulation of the ODE on 29 March becomes more consistent with the observations, especially the termination of this ODE. Thus, we suggested that this ODE at Barrow is highly associated with the air transported from the Chukotka Peninsula.

3.5 Process analysis

425 In order to study these ODEs deeper, we then applied the process analysis (PA), to estimate the contribution from each physical or chemical process to the changes of ozone and bromine species. We first show the ozone change during ODE1 caused by the overall chemistry (see Fig. 14). It can be seen that during the daytime, in most areas, ozone was formed by the chemistry the chemistry forms ozone in the presence of sunlight during the daytime in most areas. However, in places where bromine species

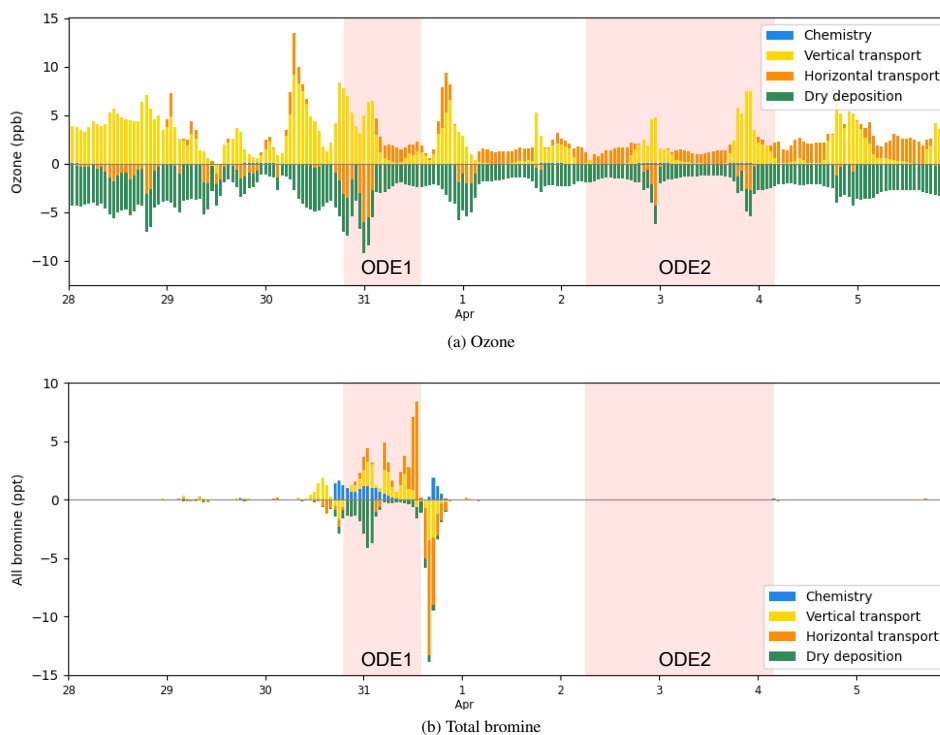


Figure 15. [The process analysis of surface ozone and bromine species \(\$\text{Br}\$, \$\text{Br}_2\$, \$\text{BrO}\$, \$\text{BrCl}\$, \$\text{HBr}\$, \$\text{HOBr}\$, \$\text{BrNO}_2\$ and \$\text{BrONO}_2\$ \) at Barrow from 28 March to 6 April, 2019.](#)

were activated ~~due to the bromine explosion mechanism, ozone was consumed by the local chemistry.~~ [the local chemistry,](#)
 430 [which is mainly dominated by the bromine chemistry, causes the decrease of ozone.](#) At 02 UTC of ~~March 30th~~ [30 March](#), the
 chemical consumption of surface ozone reached 64 ppb (see Fig. 14a). At 04 UTC when the sun ~~was setting~~ [set](#), the chemical
 influence disappeared along with the skyline of the sunset (see Fig. 14b). When [the](#) sun rose again (Fig. 14c), bromine species
 began to form again under the sunny ~~condition~~ [conditions](#), and the chemical consumption of the surface ozone reached 10 ppb
 over the Beaufort Sea. However, this strong consumption lasted only a few hours, which declined to 8 ppb at 02 UTC shown
 435 in Fig. 14(d). For the chemical contribution to the surface ozone with a finer time interval, please refer to Fig. [S9-S11](#) in the
 supplement.

In contrast to ODE1, the occurrence of ODE2 is not ~~mainly determined~~ [significantly influenced](#) by the local chemistry, so
 that the chemical contribution to the occurrence of ODE2 is negligible. Thus, we are not showing it in this paper.

We then calculated the contributions from all the physical and chemical processes to the ~~change~~ [changes](#) of ozone and
 440 bromine species at Barrow from ~~March 28th to April 6th~~ [28 March to 6 April](#), 2019, ~~shown in~~ (Fig. 15). The vertical transport

(including vertical diffusion, vertical advection and dry deposition), horizontal transport (including horizontal diffusion and horizontal advection), and dry deposition were contained.

From Fig. 15(a), it can be seen that the occurrence of ODE1 in Barrow on March 31st at Barrow on 31 March was mainly caused by the horizontal transport, which contributed to approximately 6 ppb of the ozone loss. Besides, the recovery of the ODE on March 31st was also owed to the horizontal transport. Thus, during this period, Thus, we suggested that an ozone depleted air from the ocean was horizontally advected to Barrow, leading to the ozone decline during ODE1. And the termination of ODE1 was caused due to the replenish of In contrast, the recovery of this ODE on 31 March was owed to the combined effect of the horizontal transport and the vertical transport, replenishing ozone-rich air horizontally advected from other areas. Then, during and the free atmosphere aloft into the boundary layer. With respect to ODE2 on April 2nd 2 April, the ozone loss was also found to be largely contributed by the horizontal transport. During the end of ODE2 on April 3rd, a strong vertical transport contributed approximately 5 ppb to the ozone recovery, so that the surface ozone can at the end of ODE2 on 3 April, allowing surface ozone to recover to the background level. Thus, vertical transport was primarily responsible for the recovery of ODE2 was mainly owed to the vertical transport at Barrow.

Fig. 15(b) shows the contributions of physical and chemical processes to the change of bromine species during the simulated period. It On 30 March, it was found that the variation of the bromine species on March 30th was variations of bromine species were mainly affected by the chemical process and vertical transport, vertical transport and dry deposition. The chemical process and the vertical transport caused an increase of bromine species by almost 20 approximately 4 ppt. In contrast, the vertical transport deposition contributed at most 25 ppt to the bromine loss, among which the dry deposition was predominant. This was. This is because during ODE1, the cyclone dominates dominated, leading to a strong wind and a vigorous convection within the boundary layer. As a result, the dry deposition velocities of bromine species remarkably increased was enhanced remarkably. Then, on March 31st, the bromine 31 March, bromine species were horizontally transported to Barrow, contributing approximately 8 ppb to the increase of the total bromine amount. Later, bromine species left Barrow mainly due to the horizontal transport combined effect of the horizontal transport and the vertical transport, which is consistent with the cause of the termination of ODE1 discussed above.

465 4 Conclusions and future studies

In this study, we conducted a three-dimensional simulation of ozone depletion events (ODEs) over Barrow and its surrounding areas by using a mesoscale air-quality models model, CMAQ, from March 28th to April 6th, 28 March to 6 April 2019. Several ODEs observed at Barrow were captured by the model, and two of them (ODE1 and ODE2) were analyzed thoroughly using process analysis.

470 During ODE1 occurring between ODE 1, which occurred between 30 and 31 March 30th and 31st, a cyclone that moved from the Chukchi Sea traveled to the Beaufort Sea, which provoked led to a strong wind condition along its trajectory. As a result, a large amount number of sea-salt aerosols were released from the Bering Strait, liberating active bromine due to by the bromine explosion mechanism. Then the bromine-containing air was The bromine-rich air was then carried to the Beaufort Sea

~~and induced with the movement of the cyclone, contributing to~~ a rapid depletion of ~~the~~ surface ozone over the ~~Beaufort Sea.~~
475 ~~Under the influence of horizontal transport~~ sea. Then, due to the horizontal transport of low-ozone air from the sea, a partial
ODE was observed ~~in Barrow. The at Barrow.~~ Later, the termination of this ODE was ~~also due to~~ ~~found to be caused by~~ the
horizontal advection of ozone-rich air to Barrow ~~and the vertical mixing of the air from layers aloft into the boundary layer.~~
Regarding ODE2 ~~occurring in Barrow on April 2nd~~ ~~at Barrow on 2 April~~, it was found to ~~be resulted~~ ~~result~~ from the transport of
a low-ozone center from the Arctic Sea to Barrow under the influence of a high pressure system. This ~~ozone-lacking status in~~
480 ~~low-ozone status at~~ Barrow then recovered to normal due to ~~a the~~ vertical transport of ozone-rich air from the free atmosphere.
From the vertical profiles of ozone, bromine species, and wind during these two ODEs, we found that in the presence of
a strong ~~uplifting, the ozone-lacking uplift, the low-ozone but bromine-rich~~ air can be carried to an altitude above the top
of the boundary layer, which then influenced the air in the free atmosphere. In contrast, when a stable stratification and a
temperature inversion occurred, the low-ozone status would last longer and the air containing depleted ozone ~~can~~ ~~was able to~~
485 travel further. However, as time ~~passes~~ ~~passed~~ by, under the influence of a high-pressure system, the impact of the descending
air accumulated, so that ozone in the free troposphere ~~was~~ eventually mixed into the boundary layer, ending this ODE.
A process analysis (PA) was also used to quantitatively evaluate the contributions of physical and chemical processes to
these two ODEs. It showed that the ODE1 ~~in at~~ Barrow was mainly caused by the horizontal transport, which contributed
to about 6 ppb of the ozone loss. The recovery of this ODE was ~~also~~ largely attributed to the ~~horizontal transport~~ ~~combined~~
490 ~~effect of the horizontal transport and the vertical transport.~~ However, over the sea, the ~~ozone depletion was highly contributed~~
~~by the chemical process, reaching 6-10~~ ~~chemical process significantly contributed to the ozone depletion, reaching 10~~ ppb ~~at~~
~~most.~~ The process analysis also showed that the ODE ~~occurring on April 2nd~~ ~~on 2 April~~ (i.e., ODE2) was ~~formed mainly due~~
~~to~~ ~~mainly formed by~~ the horizontal transport. In contrast, at the end stage of ODE2, a strong vertical transport contributed
approximately 5 ppb to the ozone recovery, so that the ozone recovered to the background level. Thus, the recovery of ODE2
495 was mainly owed to the vertical transport.
Although we ~~well~~ reproduced the ODEs ~~occurring during the spring~~ ~~during the springtime~~ of 2019 and analyzed the con-
tributions of ~~physicochemical processes to the ODEs, there still exist some limitations for~~ ~~physical and chemical processes to~~
~~these ODEs,~~ the present study ~~still has some limitations.~~ For instance, the heterogeneous reaction ~~rate~~ representing the bromine
explosion mechanism needs a better parameterization. ~~Besides, more observational data would help to further validate our~~
500 ~~simulations.~~ ~~In addition, simulations for other stations in Arctic are prospected to verify the~~ ~~Moreover, the overestimation of~~
~~ozone by the model needs further improvements.~~ From the study of Benavent et al. (2022), ozone depletion was suggested to
~~be strongly connected to the enhancement of iodine. Thus, the deviation between simulations and observations in the present~~
~~simulation may come from the missing iodine chemistry in the chemical mechanism of the model. In the future, we will use~~
~~a chemical mechanism including a more comprehensive halogen chemistry, which has been implemented in CMAQ 5.3 and~~
505 ~~more recent versions (i.e., CB6r3m). Furthermore, we would improve the boundary conditions used in this study and may also~~
~~enlarge the computational domain to include more observational sites in the Arctic so that the conclusions achieved in this~~
~~study can be further verified. In addition, more observational data would help to further validate our simulations.~~

Code and data availability. The code of the WRF software was obtained from https://www2.mmm.ucar.edu/wrf/users/download/get_sources.html. The code of the CMAQ software was taken from <https://github.com/USEPA/CMAQ/>. The FNL data were adopted from <https://doi.org/10.5065/D65Q4T4Z>. Outputs of CAM-Chem model for the implemented boundary conditions of CMAQ were obtained from www.acom.ucar.edu/cam-chem/cam-chem.shtml. The observational data of in-situ meteorology and ozone were provided by the Global Monitoring Laboratory (GML) (<https://gml.noaa.gov/aftp/data/barrow/>), belonging to the National Oceanic and Atmospheric Administration (NOAA). The GOME-2 satellite data of the tropospheric BrO column density were taken from <https://navigator.eumetsat.int/product/EO:EUM:DAT:0604>. The surface analysis was obtained from Weather Prediction Center (www.wpc.ncep.noaa.gov/html/sfc-zoom.php). The code for changing the boundary conditions of CMAQ can be found in <https://github.com/Simeng-unique/acp-supplements>.

Video supplement. The video supplement related to this article can be found in <https://github.com/Simeng-unique/acp-supplements>.

Author contributions. Le Cao conceived the idea of the article. Simeng Li configured and performed the computations. Simeng also revised the chemical mechanisms and wrote the paper together with Le Cao. Yicheng Gu and Yuhan Luo participated in discussions and gave valuable suggestions on the improvement of the manuscript. All the authors listed read and approved the final manuscript.

Competing interests. The authors declare that they have no conflict of interest.

Acknowledgements. Numerical calculations in this paper have been performed on the high-performance computing system in the High Performance Computing Center, Nanjing University of Information Science & Technology. The authors also like to thank Barron Henderson and Golam Sarwar from U.S. EPA sincerely for helping us dealing with ocean file, which is to be used in a future study using CMAQ v5.3.2.

Financial support. This research has been supported by the National Key Research and Development Program of China (grant no., 2022YFC3701204) and the National Natural Science Foundation of China (grant no. 41705103).

References

- AC SAF: GOME-2 Tropospheric BrO Column Data Record Release 1 - Metop, https://doi.org/10.15770/EUM_SAF_O3M_0012, 2022.
- Anderson, P. S. and Neff, W. D.: Boundary layer physics over snow and ice, *Atmospheric Chemistry and Physics*, 8, 3563–3582, <https://doi.org/10.5194/acp-8-3563-2008>, 2008.
- 530 Baek, B. and Seppanen, C.: CEMPD/SMOKE: SMOKE v4.7 Public Release (October 2019), <https://doi.org/10.5281/zenodo.3476744>, 2019.
- Barrie, L. A., Bottenheim, J. W., Schnell, R. C., Crutzen, P. J., and Rasmussen, R. A.: Ozone destruction and photochemical reactions at polar sunrise in the lower Arctic atmosphere, *Nature*, 334, 138–141, <https://doi.org/10.1038/334138a0>, 1988.
- Benavent, N., Mahajan, A. S., Li, Q., Cuevas, C. A., Schmale, J., Angot, H., Jokinen, T., Quéléver, L. L. J., Blechschmidt, A. M., Zilker, B., Richter, A., Serna, J. A., Garcia-Nieto, D., Fernandez, R. P., Skov, H., Dumitrascu, A., oes Pereira, P. S., Abrahamsson, K., Bucci, S.,
- 535 Duetsch, M., Stohl, A., Beck, I., Laurila, T., Blomquist, B., Howard, D., Archer, S. D., Bariteau, L., Helmig, D., Hueber, J., Jacobi, H.-W., Posman, K., Dada, L., Daellenbach, K. R., and Saiz-Lopez, A.: Substantial contribution of iodine to Arctic ozone destruction, *Nature Geoscience*, 15, 770–773, <https://doi.org/10.1038/s41561-022-01018-w>, 2022.
- Blechschmidt, A.-M., Richter, A., Burrows, J. P., Kaleschke, L., Strong, K., Theys, N., Weber, M., Zhao, X., and Zien, A.: An exemplary case of a bromine explosion event linked to cyclone development in the Arctic, *Atmospheric Chemistry and Physics*, 16, 1773–1788,
- 540 <https://doi.org/10.5194/acp-16-1773-2016>, 2016.
- Bottenheim, J. W. and Chan, E.: A trajectory study into the origin of spring time Arctic boundary layer ozone depletion, *Journal of Geophysical Research: Atmospheres*, 111, <https://doi.org/10.1029/2006JD007055>, 2006.
- Bottenheim, J. W., Barrie, L. A., Atlas, E., Heidt, L. E., Niki, H., Rasmussen, R. A., and Shepson, P. B.: Depletion of lower tropospheric ozone during Arctic spring: The Polar Sunrise Experiment 1988, *Journal of Geophysical Research: Atmospheres*, 95, 18 555–18 568,
- 545 <https://doi.org/10.1029/JD095iD11p18555>, 1990.
- Bottenheim, J. W., Netcheva, S., Morin, S., and Nghiem, S. V.: Ozone in the boundary layer air over the Arctic Ocean: measurements during the TARA transpolar drift 2006–2008, *Atmospheric Chemistry and Physics*, 9, 4545–4557, <https://doi.org/10.5194/acp-9-4545-2009>, 2009.
- Boylan, P., Helmig, D., Staebler, R., Turnipseed, A., Fairall, C., and Neff, W.: Boundary layer dynamics during the Ocean-
- 550 Atmosphere-Sea-Ice-Snow (OASIS) 2009 experiment at Barrow, AK, *Journal of Geophysical Research: Atmospheres*, 119, 2261–2278, <https://doi.org/10.1002/2013JD020299>, 2014.
- Buchholz, R. R., Emmon, L. K., Tilmes, S., and The CESM2 Development Team: CESM2.1/CAM-chem Instantaneous Output for Boundary Conditions, Tech. rep., UCAR/NCAR - Atmospheric Chemistry Observations and Modeling Laboratory, 10.5065/NMP7-EP60, subset used Lat: 20 to 88, Lon: -180 to -130, March 2019 - April 2019, Accessed 27 Apr 2021, 2019.
- 555 Chen, F., Janjić, Z., and Mitchell, K.: Impact of Atmospheric Surface-layer Parameterizations in the new Land-surface Scheme of the NCEP Mesoscale Eta Model, *Boundary-Layer Meteorology*, 85, 391–421, <https://doi.org/10.1023/A:1000531001463>, 1997.
- Crippa, M., Guizzardi, D., Muntean, M., Schaaf, E., Dentener, F., van Aardenne, J. A., Monni, S., Doering, U., Olivier, J. G. J., Pagliari, V., and Janssens-Maenhout, G.: Gridded emissions of air pollutants for the period 1970–2012 within EDGAR v4.3.2, *Earth System Science Data*, 10, 1987–2013, <https://doi.org/10.5194/essd-10-1987-2018>, 2018.
- 560 Crippa, M., Solazzo, E., Huang, G., and et al.: High resolution temporal profiles in the Emissions Database for Global Atmospheric Research, *Sci Data*, 7, <https://doi.org/10.1038/s41597-020-0462-2>, 2020.

- Emmons, L. K., Schwantes, R. H., Orlando, J. J., Tyndall, G., Kinnison, D., Lamarque, J.-F., Marsh, D., Mills, M. J., Tilmes, S., Bardeen, C., Buchholz, R. R., Conley, A., Gettelman, A., Garcia, R., Simpson, I., Blake, D. R., Meinardi, S., and Pétron, G.: The Chemistry Mechanism in the Community Earth System Model Version 2 (CESM2), *Journal of Advances in Modeling Earth Systems*, 12, e2019MS001882, 2020, <https://doi.org/10.1029/2019MS001882>, 2020.
- 565 EPA: Code base for the U.S. EPA's Community Multiscale Air Quality Model (CMAQ)., Tech. rep., EPA, https://github.com/USEPA/CMAQ/blob/5.2.1/CCTM/src/MECHS/cb05eh51_ae6_aq/mech_cb05eh51_ae6_aq.def, 2023.
- Fan, S.-M. and Jacob, D.: Surface ozone depletion in Arctic spring sustained by bromine reactions on aerosols, *Nature*, 359, 522–524, <https://doi.org/10.1038/359522a0>, 1992.
- 570 Gipson, G. L.: Chapter 16: Process analysis, *Science Algorithms of the EPA Models-3 Community Multiscale Air Quality (CMAQ) Modeling System*, <https://nepis.epa.gov/Exe/ZyPURL.cgi?Dockey=30003R9Y.txt>, ePA/600/R-99/030, 1999.
- Hausmann, M. and Platt, U.: Spectroscopic measurement of bromine oxide and ozone in the high Arctic during Polar Sunrise Experiment 1992, *Journal of Geophysical Research: Atmospheres*, 99, 25 399–25 413, <https://doi.org/10.1029/94JD01314>, 1994.
- Herbert, G., Green, E., Harris, J., Koenig, G., Roughton, S., and Thaut, K.: Control and Monitoring Instrumentation for the Continuous Measurement of Atmospheric CO₂ and Meteorological Variables, *Journal of Atmospheric and Oceanic Technology*, 3, 414–421, 1986a.
- 575 Herbert, G., Green, E., Koenig, G., and Thaut, K.: Monitoring instrumentation for the continuous measurement and quality assurance of meteorological observations, Tech. rep., NOAA Tech. Memo. ERL ARL-148, 1986b.
- Herbert, G., Harris, J., Bieniulis, M., and McCutcheon, J.: Acquisition and Data Management, in *CMDL Summary Report 1989*, Tech. Rep. 18, 1990.
- 580 Herbert, G., Bieniulis, M., Mefford, T., and Thaut, K.: Acquisition and Data Management Division, in *CMDL Summary Report 1993*, Tech. Rep. 22, 1994.
- Herrmann, M., Sihler, H., Frieß, U., Wagner, T., Platt, U., and Gutheil, E.: Time-dependent 3D simulations of tropospheric ozone depletion events in the Arctic spring using the Weather Research and Forecasting model coupled with Chemistry (WRF-Chem), *Atmospheric Chemistry and Physics*, 21, 7611–7638, <https://doi.org/10.5194/acp-21-7611-2021>, 2021.
- 585 Herrmann, M., Schöne, M., Borger, C., Warnach, S., Wagner, T., Platt, U., and Gutheil, E.: Ozone depletion events in the Arctic spring of 2019: a new modeling approach to bromine emissions, *Atmospheric Chemistry and Physics*, 22, 13 495–13 526, <https://doi.org/10.5194/acp-22-13495-2022>, 2022.
- Iacono, M. J., Delamere, J. S., Mlawer, E. J., Shephard, M. W., Clough, S. A., and Collins, W. D.: Radiative forcing by long-lived greenhouse gases: Calculations with the AER radiative transfer models, *Journal of Geophysical Research: Atmospheres*, 113, <https://doi.org/10.1029/2008JD009944>, 2008.
- 590 Janjić, Z. I.: The Step-Mountain Eta Coordinate Model: Further Developments of the Convection, Viscous Sublayer Turbulence Closure Schemes, *Monthly Weather Review*, 122, 927 – 945, [https://doi.org/10.1175/1520-0493\(1994\)122<0927:TSMECM>2.0.CO;2](https://doi.org/10.1175/1520-0493(1994)122<0927:TSMECM>2.0.CO;2), 1994.
- Lehrer, E., Hönninger, G., and Platt, U.: A one dimensional model study of the mechanism of halogen liberation and vertical transport in the polar troposphere, *Atmospheric Chemistry and Physics*, 4, 2427–2440, <https://doi.org/10.5194/acp-4-2427-2004>, 2004.
- 595 Liao, J., Huey, L. G., Tanner, D. J., Flocke, F. M., Orlando, J. J., Neuman, J. A., Nowak, J. B., Weinheimer, A. J., Hall, S. R., Smith, J. N., Fried, A., Staebler, R. M., Wang, Y., Koo, J.-H., Cantrell, C. A., Weibring, P., Walega, J., Knapp, D. J., Shepson, P. B., and Stephens, C. R.: Observations of inorganic bromine (HOBr, BrO and Br₂) speciation at Barrow, Alaska, in spring 2009, *Journal of Geophysical Research: Atmospheres*, 117, <https://doi.org/10.1029/2011JD016641>, 2012.

- Marelle, L., Thomas, J. L., Ahmed, S., Tuite, K., Stutz, J., Dommergue, A., Simpson, W. R., Frey, M. M., and Baladima, F.: Implementation and Impacts of Surface and Blowing Snow Sources of Arctic Bromine Activation Within WRF-Chem 4.1.1, *Journal of Advances in Modeling Earth Systems*, 13, e2020MS002391, <https://doi.org/10.1029/2020MS002391>, 2021.
- 600 McClure-Begley, A., Petropavlovskikh, I., and Oltmans, S.: NOAA Global Monitoring Surface Ozone Network, <https://doi.org/10.7289/V57P8WBF>, 2014.
- McConnell, J. C., Henderson, G. S., Barrie, L., Bottenheim, J., Niki, H., Langford, C. H., and Templeton, E. M. J.: Photochemical bromine production implicated in Arctic boundary-layer ozone depletion, *Nature*, 355, 150–152, <https://doi.org/10.1038/355150a0>, 1992.
- 605 Mefford, T., Bieniulis, M., Halter, B., and Peterson, J.: Meteorological Measurements, in CMDL Summary Report 1994 - 1995, Tech. Rep. 23, 1996.
- Mellberg, J.: Final Report Ozone Depletion by Bromine and Iodine over the Gulf of Mexico, Tech. rep., Texas Commission on Environmental Quality, 2014.
- 610 Monforti-Ferrario, F., Oreggioni, G., Schaaf, E., Guizzardi, D., Olivier, J., Solazzo, E., Lo Vullo, E., Crippa, M., Muntean, M., and Vignati, E.: Fossil CO₂ and GHG emissions of all world countries, <https://doi.org/10.2760/687800>, 2019.
- National Centers for Environmental Prediction, National Weather Service, NOAA, and U.S. Department of Commerce: NCEP GDAS/FNL 0.25 Degree Global Tropospheric Analyses and Forecast Grids, 10.5065/D65Q4T4Z, 2015.
- Oltmans, S. J.: Surface ozone measurements in clean air, *Journal of Geophysical Research: Oceans*, 86, 1174–1180, <https://doi.org/10.1029/JC086iC02p01174>, 1981.
- 615 Pesaresi, M., Florczyk, A., Schiavina, M., Melchiorri, M., and Maffeni, L.: GHS-SMOD R2019A - GHS settlement layers, updated and refined REGIO model 2014 in application to GHS-BUILT R2018A and GHS-POP R2019A, multitemporal (1975-1990-2000-2015), Tech. rep., European Commission, Joint Research Centre (JRC), <https://doi.org/10.2905/42E8BE89-54FF-464E-BE7B-BF9E64DA5218>, 2019.
- Platt, U. and Hönninger, G.: The role of halogen species in the troposphere, *Chemosphere*, 52, 325–338, [https://doi.org/10.1016/S0045-6535\(03\)00216-9](https://doi.org/10.1016/S0045-6535(03)00216-9), naturally Produced Organohalogen, 2003.
- 620 Platt, U. and Lehrer, E.: Arctic tropospheric ozone chemistry - ARCTOC : results from field, laboratory and modelling studies : final report of the EU project Contract No EV5V-V-CT93-0318(DTEF), Luxembourg, 1997.
- Ranchar, J. and Kritz, M. A.: Diurnal fluctuations of Br and I in the tropical marine atmosphere, *Journal of Geophysical Research: Oceans*, 85, 5581–5587, <https://doi.org/10.1029/JC085iC10p05581>, 1980.
- 625 Sarwar, G., Gantt, B., Schwede, D., Foley, K., Mathur, R., and Saiz-Lopez, A.: Impact of Enhanced Ozone Deposition and Halogen Chemistry on Tropospheric Ozone over the Northern Hemisphere, *Environmental Science & Technology*, 49, 9203–9211, <https://doi.org/10.1021/acs.est.5b01657>, 2015.
- Seinfeld, J. H. and Pandis, S. N.: *Atmospheric Chemistry and Physics: From Air Pollution to Climate Change*, John Wiley & Sons, third edition edn., 2016.
- 630 Sharma, S., Barrie, L., Magnusson, E., Brattström, G., Leaitch, W., Steffen, A., and Landsberger, S.: A Factor and Trends Analysis of Multidecadal Lower Tropospheric Observations of Arctic Aerosol Composition, Black Carbon, Ozone, and Mercury at Alert, Canada, *Journal of Geophysical Research: Atmospheres*, 124, 14 133–14 161, <https://doi.org/https://doi.org/10.1029/2019JD030844>, 2019.
- Sherwen, T., Evans, M. J., Carpenter, L. J., Andrews, S. J., Lidster, R. T., Dix, B., Koenig, T. K., Sinreich, R., Ortega, I., Volkamer, R., Saiz-Lopez, A., Prados-Roman, C., Mahajan, A. S., and nez, C. O.: Iodine’s impact on tropospheric oxidants: a global model study in GEOS-Chem, *Atmospheric Chemistry and Physics*, 16, 1161–1186, <https://doi.org/10.5194/acp-16-1161-2016>, 2016.
- 635

- Simpson, W. R., von Glasow, R., Riedel, K., Anderson, P., Ariya, P., Bottenheim, J., Burrows, J., Carpenter, L. J., Frieß, U., Goodsite, M. E., Heard, D., Hutterli, M., Jacobi, H.-W., Kaleschke, L., Neff, B., Plane, J., Platt, U., Richter, A., Roscoe, H., Sander, R., Shepson, P., Sodeau, J., Steffen, A., Wagner, T., and Wolff, E.: Halogens and their role in polar boundary-layer ozone depletion, *Atmospheric Chemistry and Physics*, 7, 4375–4418, <https://doi.org/10.5194/acp-7-4375-2007>, 2007.
- 640 Skamarock, W. C., Klemp, J. B., and J. Dudhia, e. a.: A Description of the Advanced Research WRF Version 3, Tech. rep., University Corporation for Atmospheric Research, <https://doi.org/http://dx.doi.org/10.5065/D68S4MVH>, 2008.
- Steffen, A., Douglas, T., Amyot, M., Ariya, P., Aspö, K., Berg, T., Bottenheim, J., Brooks, S., Cobbett, F., Dastoor, A., Dommergue, A., Ebinghaus, R., Ferrari, C., Gardfeldt, K., Goodsite, M. E., Lean, D., Poulain, A. J., Scherz, C., Skov, H., Sommar, J., and Temme, C.: A synthesis of atmospheric mercury depletion event chemistry in the atmosphere and snow, *Atmospheric Chemistry and Physics*, 8, 1445–1482, <https://doi.org/10.5194/acp-8-1445-2008>, 2008.
- 645 Stull, R. B.: *An Introduction to Boundary Layer Meteorology*, Springer, Dordrecht, <https://doi.org/10.1007/978-94-009-3027-8>, 1988.
- Swanson, W., Graham, K. A., Halfacre, J. W., Holmes, C. D., Shepson, P. B., and Simpson, W. R.: Arctic Reactive Bromine Events Occur in Two Distinct Sets of Environmental Conditions: A Statistical Analysis of 6 Years of Observations, *Journal of Geophysical Research: Atmospheres*, 125, e2019JD032139, <https://doi.org/10.1029/2019JD032139>, 2020.
- 650 Thomas, J. L., Stutz, J., Lefer, B., Huey, L. G., Toyota, K., Dibb, J. E., and von Glasow, R.: Modeling chemistry in and above snow at Summit, Greenland – Part 1: Model description and results, *Atmospheric Chemistry and Physics*, 11, 4899–4914, <https://doi.org/10.5194/acp-11-4899-2011>, 2011.
- Thomas, J. L., Dibb, J. E., Huey, L. G., Liao, J., Tanner, D., Lefer, B., von Glasow, R., and Stutz, J.: Modeling chemistry in and above snow at Summit, Greenland – Part 2: Impact of snowpack chemistry on the oxidation capacity of the boundary layer, *Atmospheric Chemistry and Physics*, 12, 6537–6554, <https://doi.org/10.5194/acp-12-6537-2012>, 2012.
- 655 Thompson, G., Field, P. R., Rasmussen, R. M., and Hall, W. D.: Explicit Forecasts of Winter Precipitation Using an Improved Bulk Microphysics Scheme. Part II: Implementation of a New Snow Parameterization, *Monthly Weather Review*, 136, 5095 – 5115, <https://doi.org/10.1175/2008MWR2387.1>, 2008.
- Tiedtke, M.: A Comprehensive Mass Flux Scheme for Cumulus Parameterization in Large-Scale Models, *Monthly Weather Review*, 117, 1779 – 1800, [https://doi.org/10.1175/1520-0493\(1989\)117<1779:ACMFSF>2.0.CO;2](https://doi.org/10.1175/1520-0493(1989)117<1779:ACMFSF>2.0.CO;2), 1989.
- 660 US EPA Office of Research and Development: CMAQ, <https://doi.org/10.5281/zenodo.1212601>, For up-to-date documentation, source code, and sample run scripts, please clone or download the CMAQ git repository available through GitHub: <https://github.com/USEPA/CMAQ/tree/5.2.1>, 2018.
- US EPA Office of Research and Development: CMAQ, <https://doi.org/10.5281/zenodo.4081737>, For up-to-date documentation, source code, and sample run scripts, please clone or download the CMAQ git repository available through GitHub: <https://github.com/USEPA/CMAQ>, 2020.
- 665 von Glasow, R. and Crutzen, P.: 5.2 - Tropospheric Halogen Chemistry, in: *Treatise on Geochemistry (Second Edition)*, edited by Holland, H. D. and Turekian, K. K., pp. 19–69, Elsevier, Oxford, second edition edn., <https://doi.org/10.1016/B978-0-08-095975-7.00402-2>, 2014.
- Wennberg, P. O.: Bromine Explosion, *Nature*, 397, 299–301, <https://doi.org/10.1038/16805>, 1999.
- 670 Yang, X., Pyle, J. A., and Cox, R. A.: Sea salt aerosol production and bromine release: Role of snow on sea ice, *Geophysical Research Letters*, 35, <https://doi.org/10.1029/2008GL034536>, 2008.
- Yang, X., Pyle, J. A., Cox, R. A., Theys, N., and Van Roozendael, M.: Snow-sourced bromine and its implications for polar tropospheric ozone, *Atmospheric Chemistry and Physics*, 10, 7763–7773, <https://doi.org/10.5194/acp-10-7763-2010>, 2010.

- 675 Yang, X., Frey, M. M., Rhodes, R. H., Norris, S. J., Brooks, I. M., Anderson, P. S., Nishimura, K., Jones, A. E., and Wolff, E. W.: Sea salt aerosol production via sublimating wind-blown saline snow particles over sea ice: parameterizations and relevant microphysical mechanisms, *Atmospheric Chemistry and Physics*, 19, 8407–8424, <https://doi.org/10.5194/acp-19-8407-2019>, 2019.
- Yarwood, G., Jung, J., Nopmongcol, O., and Emery, C.: Final Report Improving CAMx Performance in Simulating Ozone Transport from the Gulf of Mexico, Tech. rep., Texas Commission on Environmental Quality, 2012.
- 680 Zeng, T., Wang, Y., Chance, K., Browell, E. V., Ridley, B. A., and Atlas, E. L.: Widespread persistent near-surface ozone depletion at northern high latitudes in spring, *Geophysical Research Letters*, 30, <https://doi.org/10.1029/2003GL018587>, 2003.
- Zeng, T., Wang, Y., Chance, K., Blake, N., Blake, D., and Ridley, B.: Halogen-driven low-altitude O₃ and hydrocarbon losses in spring at northern high latitudes, *Journal of Geophysical Research: Atmospheres*, 111, <https://doi.org/10.1029/2005JD006706>, 2006.